Annihilation decays of bound states at the LHC

Yevgeny Kats and Matthew D. Schwartz

Department of Physics, Harvard University,
Cambridge, MA 02138, U.S.A.

E-mail: kats@physics.harvard.edu, schwartz@physics.harvard.edu

ABSTRACT: At the Large Hadron Collider, heavy particles may be produced in pairs close to their kinematic threshold. If these particles have strong enough attractive interactions they may form bound states. Consequently, the bound states may decay through annihilation back into the standard model. Such annihilation decays have the potential to provide much information about the bound particles, such as their mass, spin, or charges, in a manner completely complementary to standard single particle cascade decays. Many of the signatures, such as dijet resonances, will be challenging to find, but may be extremely helpful in unraveling the nature of the new physics. In the standard model, the only novel annihilation decays would be for toponium; these will be hard to see because of the relatively large width of the top quark itself. In models with supersymmetry, marginally visible annihilation decays may occur for example, from bound states of gluinos to dijets or tops. If new particles are bound through forces stronger than QCD, annihilation decays may even be the discovery mode for new physics. This paper presents various theoretical results about bound states and then addresses the practical question of whether any of their annihilation decays can be seen at the LHC.

Contents

1 Introduction

It will undoubtedly be much easier to conclude that the LHC has found new physics than to determine what that new physics is. Many of the most well-motivated models have signatures such as events with a large number of jets and missing energy. While there is little background from the standard model for these signatures, the difficultly of sorting out which jet corresponds to which parton, working out the underlying topologies, reconstructing the intermediate masses, and isolating the relevant couplings may be an insurmountable challenge. Special cases, for example, with multiple leptons, will make things easier, but determining couplings and masses for strongly interacting particles may require the precision of a next-generation machine. With no such machine on the horizon, it is therefore imperative to consider other ways in which parameters of the underlying Lagrangian may be extracted from data at the LHC. In this paper, we consider one often neglected possibility: massive, strongly interacting particles that are produced in pairs can form bound states which then annihilate back into the standard model. Such annihilation decays are subject to an entirely different set of systematics than standard cascade decays, and therefore, if they can be seen, provide the possibility of generating entirely complementary information about the underlying physics.

Bound states exist when the potential between the particles is attractive, with a binding energy that is larger than the particle's intrinsic width. If the states are too strongly bound, such as through new beyond-the-standard model (BSM) forces, we may never see the constituent particles on their own, that is to say, the bound states will look just like resonances. On the other extreme, if the binding energy is much smaller than the width, the equivalent of bound state production and annihilation is simply virtual pair production, with little evidence of resonance behavior over the continuum. We are interested in the intermediate regime, where the particles sometimes bind and annihilate, and other times have single particle decays, since this is when the two complementary types of signatures can be available. Conveniently, this happens fairly generically if the particles are bound through the strong force SU(3) of the standard model and the single particle decays only go through off-shell intermediate states. In particular, it happens for many standard BSM scenarios, where the bound states will typically amount to a few percent of the cross section of the pair production processes.

If the products of annihilation decays can be detected and distinguished from the background, they will provide a wealth of information. For example, the location of the peak in the invariant mass distribution of the annihilation products can lead to mass measurements more precise than those from cascade decays with missing energy. The spins of the possible bound states are determined by the properties of the constituent particles. The overall production and annihilation rates are also sensitive to the color and spins of the particles.

We begin in section 2 with a discussion of bound states of the top quark. Although we will conclude that toponium is practically invisible at the LHC, this section introduces some of the formalism for studying bound states that we will use in other sections. We proceed, in section 3 to look at beyond-the-standard model examples. While the same basic ideas

apply to any model of new physics with pair-produced colored particles, to be concrete we will discuss mostly bound states of color-adjoint fermions, such as gluinos in the minimal supersymmetric standard model (MSSM). When a gluino pair is produced close to threshold, it can form a bound state, called gluinonium [1–3]. General features of the gluinonium production cross section and annihilation rates, including various perturbative corrections, have been studied in [4–9]. Applying these results, we will find that annihilation decays of gluinonium are relevant for realistic SUSY spectra such as some of the SPS benchmark points [10], as well as for more exotic scenarios such as those with a gluino LSP [11, 12] or split supersymmetry [13]. Some possibly observable final states from annihilation decays of gluinonium include dijets and $t\bar{t}$ pairs. In section 4, we study these decay modes through Monte Carlo simulation, and compare them to the relevant backgrounds. In section 5 we discuss bound states of particles with other spins, color representations and charges than the gluino. These include squark-(anti)squark and squark-gluino bound states in the MSSM. In section 6 we explore what happens when the particles are bound by a new force that is stronger than $\mathrm{SU(3)_{QCD}}$. Section 7 summarizes the various results we find, and concludes.

2 Wide bound states: toponium

A reasonable place to start is a review of the bound state formalism for heavy colored particles in the standard model. In order to study bound states using perturbation theory, the mass of the particles which bind should be larger than Λ_{QCD}. Bound states of charm quarks (charmonium, such as J/ψ) and bottom quarks (bottomonium, such as Υ) have been well-measured and are well-understood theoretically. Bound states of the top-quark, toponia, have been studied theoretically as well, but have not yet been seen in colliders. In this section, we will review what is known about toponia, and consider the prospects for their observation. We will see that the $t\bar{t}$ invariant mass spectrum does show evidence of binding, but the top quark width is too large to allow for any detectable amount of annihilation decays at the LHC. In the next sections, we will study more general non standard-model scenarios in which annihilation decays are more relevant.

2.1 Bound state formalism

The appropriate way to study the formation and decay of bound states is with non-relativistic QCD (NRQCD). At high energy, relevant to the production of massive particles at colliders, QCD is a perturbative field theory. Therefore, at leading order, the dynamics of a pair of colored particles of mass $m \gg \Lambda_{\mathrm{QCD}}$ can be described by the single-gluon exchange potential which has the form

$$V(r) = -C\frac{\overline{\alpha}_s}{r}\,. \tag{2.1}$$

The color factor C is obtained by evaluating the product of SU(3) generators. Labeling the particles 1 and 2, this product is $-T_1^a T_2^a = \frac{1}{2}((T_1^a)^2 + (T_2^a)^2 - (T_1^a + T_2^a)^2)$, which leads to

$$C = \frac{1}{2}\left(C_1 + C_2 - C_{(12)}\right)\,, \tag{2.2}$$

where C_1 and C_2 are the quadratic Casimirs for the two particles and $C_{(12)}$ that for the bound state.

The coupling constant in eq. (2.1) is defined as

$$\overline{\alpha}_s \equiv \alpha_s(a_0^{-1}),\qquad (2.3)$$

where $a_0 = (\frac{1}{2}C\overline{\alpha}_s m)^{-1}$ is the Bohr radius of the bound states. This notation is chosen to emphasize that the appropriate scale at which α_s should be evaluated in the Schrödinger equation is associated with typical momentum transfers relevant for the binding, $\mu \sim a_0^{-1}$, as opposed to the much higher energies $\mu \sim m$ which are relevant for the hard scattering production and annihilation processes. Since $\overline{\alpha}_s$ will eventually be raised to the third power, this can lead to a factor of 2 or more in the overall rate. Note that the color factor C depends on the color representation of the bound states and therefore there is a weak dependence in $\overline{\alpha}_s$ as well. Other quantities, such as the binding energy, will also depend on the representations, and to keep the notation concise, we will generally leave this dependence implicit.

When the binding particle's intrinsic width Γ is not negligible compared to the binding energy, it must be included in the Schrödinger equation. We will see that this is in fact the case for the top quark. The spectral density comprising the bound state resonances is contained in the Green's function solving

$$\left[-\frac{\nabla^2}{m} + V(r) - (E + i\Gamma) \right] G(\mathbf{x}, E) = \delta^{(3)}(\mathbf{x}),\qquad (2.4)$$

where $E = \sqrt{\hat{s}} - 2m$ is the energy from the scattering event available to the system. The bound states are produced from incoming partons with momenta $\mathbf{k}$ which correspond to much shorter wavelengths than the distance over which the bound state wavefunctions have support. Therefore, the production process probes this Green's function at effectively a single point and all we really need for the collider physics applications is $G(\mathbf{0}, E)$. For example, by the optical theorem the partonic production cross section including bound state effects is

$$\hat{\sigma}(\hat{s}) = \frac{4\pi}{m^2\beta} \operatorname{Im} G(\mathbf{0}, E)\, \hat{\sigma}_0(\hat{s}),\qquad (2.5)$$

where $\beta = \sqrt{1 - 4m^2/\hat{s}}$ is the velocity of the two particles in the center-of-mass frame and $\hat{\sigma}_0$ is the pair production cross section without including any binding effects. We can also use $G(\mathbf{0}, E)$ as a propagator for the bound states, for example in computing matrix elements for the annihilation processes.

For zero angular momentum, the solution for the Green's function is [14]

$$G(\mathbf{0}, E) = -\frac{m^2}{4\pi} \left[\sqrt{-\frac{E + i\Gamma}{m}} - C\overline{\alpha}_s \ln\left(\frac{|C|\overline{\alpha}_s}{2} \sqrt{-\frac{m}{E + i\Gamma}} \right) \right.$$
$$\left. -\frac{2}{\sqrt{m}} \sum_{n=1}^{\infty} \frac{E_n}{\sqrt{-(E + i\Gamma)} - \operatorname{sign}(C)\sqrt{E_n}} \right].\quad (2.6)$$
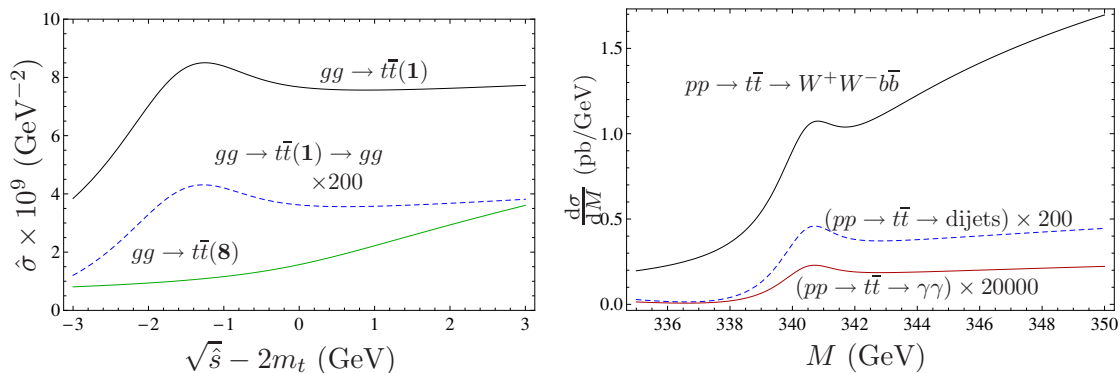
Figure 1. Near threshold $t\bar{t}$ production. The left panel shows the partonic cross section, separated by color, with the rate for annihilation decays scaled by 200. The right panel shows the physical cross section for $t\bar{t}$ production at the LHC (14 TeV). The rates for annihilation decays into dijets and $\gamma\gamma$ are shown, scaled by factors of 200 and 20000, respectively.

Here $E_n = E_b/n^2$ are the energies of the radial excitations of the ground state whose binding energy is given by

$$E_b = \frac{1}{4} C^2 \overline{\alpha}_s^2 m \,. \tag{2.7}$$

This solution encodes the resummation of Coulomb gluons to all orders in $\overline{\alpha}_s$. Further precision can be achieved with the inclusion of higher order corrections to the Coulomb potential (see, e.g., [15, 16] and references therein).

We give further details of the bound states formalism with finite width, including expressions for the production and decay rates in terms of $G(\mathbf{0}, E)$, in appendix A. The annihilation decays will really only be relevant for narrow width, where the formulas simplify. The formulas in the narrow width approximation are discussed both in appendix A and in section 3 of the main text.

2.2 Toponium

For the case of a $t\bar{t}$ pair, like for the other quarkonia, the color decomposition

$$\mathbf{3} \otimes \overline{\mathbf{3}} = \mathbf{1} \oplus \mathbf{8} \tag{2.8}$$

shows that toponium can be a color singlet or a color octet. Then

$$C_{\mathbf{1}} = C_F = \frac{4}{3} \,, \qquad C_{\mathbf{8}} = C_F - \frac{C_A}{2} = -\frac{1}{6} \,. \tag{2.9}$$

Thus, the singlet has an attractive potential while the octet does not. The top quark's intrinsic width is $\Gamma_t = 1.3\,\text{GeV}$ which is of the same order as its binding energy $E_b = \frac{1}{4} C_F^2 \overline{\alpha}_s^2 m_t = 1.5\,\text{GeV}$, so we must include the width in the toponium production.

The cross section for $t\bar{t}$ production in the color singlet and color octet configurations is shown in the first panel of figure 1. Since the octet potential is repulsive, it has no resonance behavior. The singlet configuration shows evidence for a resonance, but because of the large width of the top, the would-be bound state merges with the $t\bar{t}$ continuum.

The rate for annihilation decays of the bound state, the color singlet, is small and has to be scaled by a factor of 200 to appear on the same plot. This can be seen analytically in the (poor) approximation of a narrow toponium, where the rate of the annihilation process $(t\bar{t}) \rightarrow gg$ is [17]

$$\Gamma_{(t\bar{t})\rightarrow gg} = \frac{64}{81}\alpha_s^2 \overline{\alpha}_s^3 m_t \simeq 4 \times 10^{-3} \text{ GeV} \simeq 2 \times 10^{-3} \cdot 2\Gamma_t . \qquad (2.10)$$

Most of the production cross section corresponds to processes that end up in the weak decays of the tops, but there are also tiny branching ratios into the various annihilation channels. The physical cross sections times branching ratios for $t\bar{t}$ at the LHC (14 TeV) are shown in the second panel of figure 1. Higher-order QCD corrections to the production rate (but not the annihilation processes) have been studied recently in [16, 18], but we do not take them into account for our estimates.

In order to find evidence for binding, it is natural to search for the resonance behavior in the invariant mass of the decay products. It is also possible to search for the onset of the continuum contribution which looks like a step in the invariant mass distribution. In any case, the challenge is to find a subtle feature with a width of order $\sim 1\,\text{GeV}$ on top of a smooth continuum. In terms of overall rates, the best place to look for evidence of toponium might be in the reconstructed invariant mass spectrum from the weak decay products. However, because the reconstruction of tops is in itself full of uncertainties, and because of the radiation broadening of the hadronic part of the top-decay final states, this is not a promising direction to finding a subtle 1 GeV wide feature. The dijet annihilation decay signal is similarly hopeless. A slightly more promising channel, at least in terms of resolution, might have been the annihilation of toponium into photons, which has branching ratio of $(8/9)(\alpha/\alpha_s)^2 \simeq 0.005$ relative to the annihilation into dijets [17]. However, for this decay mode $\mathrm{d}\sigma/\mathrm{d}M \simeq 0.01\,\text{fb/GeV}$ which leads to too few signal events, especially compared to the standard model background which has $\mathrm{d}\sigma/\mathrm{d}M \simeq 1\,\text{fb/GeV}$. Similar conclusions have been reached in the limit of narrow toponium in the past [19–21].

We have seen that there are two main difficulties in finding toponium. The first is that the rate for annihilation decays is small, of order 0.2% of the production rate. The second is that the large width of the top prevents the resonance from being seen on top of the continuum background. Instead of showing a resonance shape, the annihilation decays of toponium into dijets produce a signal which merges smoothly with the continuum. Both of these problems would be ameliorated if the top had a smaller intrinsic width. Figure 2 shows what happens to the production and annihilation decay rates as the top quark width Γ_t is decreased. First note from the first panel that the resonance becomes much sharper for smaller width. Not only does the bound state become well-defined but its first radial excitations become visible too. Thus the distinction from the continuum in any decay mode will be sharper. Second, note from the second plot the relative importance of the annihilation decays of the resonance compared to the continuum. Of course, the top width is fixed, and known. But there are beyond the standard model scenarios which have phenomenology similar to a narrow top. One example is bound states of gluinos, gluinonium, to which we now turn.
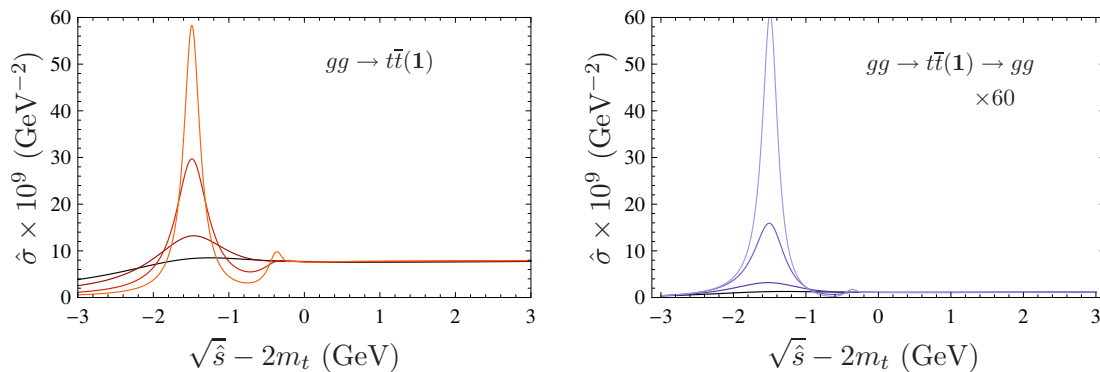
Figure 2. Varying the top width. On the left is the $t\bar{t}$ color singlet partonic production cross section and on the right is the rate for annihilation decays. The lowest curves correspond to the real top, as in figure 1, and the others, from bottom to top, have the top width decreased by factors of 2, 5 and 10. Of note are both the appearance of the bound states as well-defined resonances, and the relative fraction of annihilation decays coming from resonance region.

3   Narrow bound states: gluinonium

Having found that toponium is practically impossible to see at the LHC, let us consider in what situation bound states of colored particles might be detectable. We saw in figure 2 that the strength of the annihilation decay signal is enhanced when the single particle width is decreased. If we can neglect the particle's intrinsic width in the bound state formalism, the decay of a resonance can be simply expressed in terms of its wavefunction $\psi(\mathbf{x})$. The relevant rates are then

$$\Gamma_{\rm ann} \sim \frac{\alpha_s^2}{m^2} |\psi(\mathbf{0})|^2 \sim \alpha_s^2 \overline{\alpha}_s^3 m \,, \qquad E_b \sim \overline{\alpha}_s^2 m \,. \tag{3.1}$$

So $\Gamma_{\rm ann}/E_b \sim \alpha_s^2 \overline{\alpha}_s \ll 1$. Thus, bound states in this situation will be very narrow compared to the binding energy, like in figure 2.

As a canonical example, we will now consider bound states of gluinos, gluinonia. We will return to other cases in sections 5 and 6. Unlike the top whose properties we know, the gluino has, minimally, two free parameters: its mass $m_{\tilde{g}}$ and its width $\Gamma_{\tilde{g}}$. In many scenarios the gluino decays to a squark and a quark, with a decay rate scaling like

$$\Gamma_{\tilde{g}} \sim \alpha_s m_{\tilde{g}} \,. \tag{3.2}$$

This leads to $\Gamma_{\tilde{g}} \sim E_b$ and the gluinonium will be broad like the toponium. However, if these two-body decays are kinematically forbidden, which happens when all of the squarks are heavier than the gluino, the gluino can only decay through off-shell intermediate states (see [22, 23] for detailed studies of the various possible decay modes in this situation). In this case, the decay rate is significantly suppressed. For example, if the dominant decay mode is to quarks and a chargino or neutralino through an off-shell squark, the rate will scale like

$$\Gamma_{\tilde{g}} \sim \frac{\alpha_{\rm em} \alpha_s m_{\tilde{g}}}{16\pi \sin^2 \theta_W} \left(\frac{m_{\tilde{g}}}{m_{\tilde{q}}} \right)^4 \,. \tag{3.3}$$

In principle, this can be as small as one likes if the squarks are heavy, which enhances the fraction of annihilation decays. Since the rate goes as the fourth power of $m_{\tilde{g}}/m_{\tilde{q}}$, the squarks only need to be slightly heavier than the gluinos to saturate the rate for annihilation decays.

Keep in mind, for the annihilation decays to occur, the gluinos have to bind, which only happens near threshold. If the gluinos are produced with relativistic speeds, they still undergo single-particle decays rather than annihilating. In the case where the squarks are completely decoupled like in split supersymmetry [13], the relativistic gluinos may even form bound states with standard model particles, for example, forming R-hadrons (see, e.g., [11, 12, 24, 25]). Such exotic phenomenology is largely irrelevant to the cross section for annihilation decays in the resonance region, which is the place to look for gluinonia.

3.1 Narrow gluinonia

Since we will be interested in the limit $\Gamma_{\tilde{g}}, \Gamma_{\mathrm{ann}} \ll E_b$, we can use the narrow width approximation to simplify the bound-state formalism. In the narrow width limit, the production and annihilation of the bound states are determined by finding the energy eigenstates of the Schrödinger equation from the potential (2.1). The solutions are then wavefunctions $\psi(\mathbf{x})$, analogous to the wavefunctions of the hydrogen atom. For S-waves, these are simply functions of the radial coordinate: $\psi_n(\mathbf{x}) = \frac{1}{2\sqrt{\pi}} R_n(r)$, where n is the radial quantum number. In terms of the formalism of section 2, below the kinematic pair-production threshold, the imaginary part of the Green's function reduces to

$$\mathrm{Im}\, G(\mathbf{0}) = \pi \sum_n |\psi_n(\mathbf{0})|^2\ \delta(E + E_n)\,. \tag{3.4}$$

The short-distance part of the bound state production process is determined by the same matrix element $\mathcal{M}_0$ that describes the production of the constituent particles in the continuum. The matrix element for binding is given by [26, 27]

$$\mathcal{M}_{\mathrm{bound}} = \sqrt{\frac{2}{M}}\, \psi(\mathbf{0})\, \mathcal{M}_0\,, \tag{3.5}$$

where $M \simeq 2m$ is the mass of the bound state. Note that, although the continuum production rate vanishes at threshold $\sqrt{\hat{s}} = 2m$, this is due to phase space; the matrix element $\mathcal{M}_0$ at threshold is finite.

For identical particles, a factor of $1/2$ needs to be added in (3.5) and the wave function needs to satisfy an appropriate (anti)symmetry condition. For an S-wave spin-0 color-symmetric (or spin-1 color-antisymmetric) bound state of two gluinos (identical fermions), we should take the spatial part as

$$\psi_{\tilde{g}\tilde{g}}(\mathbf{x}) = \frac{1}{\sqrt{2}}\left[\psi(\mathbf{x}) + \psi(-\mathbf{x})\right] = \sqrt{2}\,\psi(\mathbf{x})\,. \tag{3.6}$$

These factors result in an overall factor of $1/2$ in the bound state production and annihilation rates. Following the convention in the literature, $\psi(\mathbf{x})$ in our expressions will still be normalized as in the hydrogen atom, while the extra factor of $1/2$ will be included explicitly in the prefactor.

The binding energy, Bohr radius, and the wavefunction at $\mathbf{x} = 0$ for the ground state are given by

$$E_b = \frac{C^2 \overline{\alpha}_s^2 m}{4}, \qquad a_0 = \frac{2}{C \overline{\alpha}_s m}, \qquad |\psi(\mathbf{0})|^2 = \frac{1}{\pi a_0^3} = \frac{C^3 \overline{\alpha}_s^3 m^3}{8\pi}. \qquad (3.7)$$

As before, we have made a notational distinction for the strong coupling constant evaluated at scales relevant for the binding $\overline{\alpha}_s \equiv \alpha_s(a_0^{-1})$ and the strong coupling scale relevant for the production, $\alpha_s = \alpha_s(m)$. To get a feel for the sizes of the quantities in (3.7), we can try $C = 3$ and $m = 300\,\mathrm{GeV}$, giving $E_b \simeq 11\,\mathrm{GeV}$, $1/a_0 \simeq 56\,\mathrm{GeV}$ and $|\psi(\mathbf{0})|^2 \simeq (40\,\mathrm{GeV})^3$.

Excited states are much less important than the ground state. The radial excitations have wavefunctions which at $\mathbf{x} = 0$ are given by $\psi_n(\mathbf{0}) = \psi(\mathbf{0})/n^{3/2}$, so their decay rates and cross sections are suppressed by $1/n^3$. All angular-excited states have $\psi(\mathbf{0}) = 0$, so their rates depend on the derivative of $\psi(\mathbf{x})$ with respect to the radial coordinate. These rates are then proportional to $|\psi'(\mathbf{0})|^2/m^2 \sim \overline{\alpha}_s^5 m^3$ rather than $|\psi(\mathbf{0})|^2 \sim \overline{\alpha}_s^3 m^3$ [27], which suppresses their decay rates and production cross sections by a factor of $\overline{\alpha}_s^2$ compared to the ground states. For this reason, we will only consider S-wave gluinonia. However P-wave gluinonia have been mentioned in the context of diffractive processes in [28, 29]. Note also that because their annihilation rates are suppressed, they can be corrected at the leading order by subleading terms in NRQCD. For example, in quarkonia, P states can have small admixtures of states that are made of a $q\overline{q}$ pair in an S color-octet state + a gluon [30].

The color representation of a pair of gluinos can be one of the following:

$$\mathbf{8} \otimes \mathbf{8} = \mathbf{1_S} \oplus \mathbf{8_S} \oplus \mathbf{8_A} \oplus \mathbf{10_A} \oplus \overline{\mathbf{10}}_{\mathbf{A}} \oplus \mathbf{27_S}. \qquad (3.8)$$

Here $\mathbf{S}$ and $\mathbf{A}$ subscripts refer to whether the wavefunction is symmetric or anti-symmetric in color. Based on (2.2), the color factors are

$$C_{\mathbf{1}} = C_A = 3, \qquad C_{\mathbf{8_S}} = C_{\mathbf{8_A}} = \frac{1}{2} C_A = \frac{3}{2}, \qquad C_{\mathbf{10}} = C_{\overline{\mathbf{10}}} = 0, \qquad C_{\mathbf{27}} = -1, \quad (3.9)$$

so the potential is attractive for $\mathbf{1}$, $\mathbf{8_S}$ and $\mathbf{8_A}$, zero for $\mathbf{10}$ and $\overline{\mathbf{10}}$, which are not produced at leading order [31], and repulsive for $\mathbf{27}$. Note that the color factors are raised to the third power in the expression for $|\psi(\mathbf{0})|^2$ in (3.7), and this can make a large difference in the cross section. It enhances the color singlet production over the color octet by a factor of 8. S-wave bound states exist for all the three attractive representations. Since the gluinos are identical spin-$\frac{1}{2}$ Majorana fermions, the color-symmetric states must be pseudoscalars ($J^{\mathrm{PC}} = 0^{-+}$)

$$\left| {}^1S_0(\mathbf{1}) \right\rangle = \frac{1}{\sqrt{8}} \delta_{ab}, \qquad \left| {}^1S_0(\mathbf{8_S}) \right\rangle_c = \sqrt{\frac{3}{5}}\, d_{abc} \qquad (3.10)$$

and the color-antisymmetric state must be a vector ($J^{PC} = 1^{--}$)

$$\left| {}^3S_1(\mathbf{8_A}) \right\rangle_c = \frac{1}{\sqrt{3}}\, f_{abc}, \qquad (3.11)$$

where ${}^{2S+1}L_J$ describes the rotational quantum numbers.

3.2 Annihilation decays

The gluinonia with different spins will have different annihilation modes, so let us consider the pseudoscalar and vector bound states separately. Pseudoscalar gluinonia in either the color singlet, **1**, or adjoint, **8$_\mathbf{S}$**, representation will annihilate predominantly into two gluons via the diagrams A and Ã in figure 3. Including also the normalizations from (3.5), (3.6) and (3.10), the resulting rates are [1, 2, 7]

$$\Gamma(\mathbf{1} \to gg) = \frac{18\pi\alpha_s^2}{m_{\tilde{g}}^2} \left|\psi_\mathbf{1}(\mathbf{0})\right|^2 = \frac{243}{4}\alpha_s^2\overline{\alpha}_s^3 m_{\tilde{g}}\,, \tag{3.12}$$

and [7][1]

$$\Gamma(\mathbf{8_S} \to gg) = \frac{9\pi\alpha_s^2}{2m_{\tilde{g}}^2} \left|\psi_\mathbf{8_S}(\mathbf{0})\right|^2 = \frac{243}{128}\alpha_s^2\overline{\alpha}_s^3 m_{\tilde{g}}\,. \tag{3.13}$$

The pseudoscalar gluinonia can also decay into quarks via diagrams B and B̃ in figure 3. The annihilation decay to light $q\overline{q}$ pairs is suppressed by the quark masses by chirality considerations. However, decays to $t\overline{t}$ may have a reasonable rate [5, 9]. The branching ratio for the **1** gluinonium is [9]

$$\frac{\Gamma(\mathbf{1} \to t\overline{t})}{\Gamma(\mathbf{1} \to gg)} = \frac{16}{27}\sqrt{1 - \frac{m_t^2}{m_{\tilde{g}}^2}} \frac{m_t^2 m_{\tilde{g}}^2}{\left(m_{\tilde{g}}^2 + m_{\tilde{t}}^2 - m_t^2\right)^2} \tag{3.14}$$

assuming that both stops have the same mass $m_{\tilde{t}}$. For the **8$_\mathbf{S}$** gluinonium we similarly find

$$\frac{\Gamma(\mathbf{8_S} \to t\overline{t})}{\Gamma(\mathbf{8_S} \to gg)} = \frac{20}{27}\sqrt{1 - \frac{m_t^2}{m_{\tilde{g}}^2}} \frac{m_t^2 m_{\tilde{g}}^2}{\left(m_{\tilde{g}}^2 + m_{\tilde{t}}^2 - m_t^2\right)^2}\,. \tag{3.15}$$

For $m_{\tilde{q}} \sim m_{\tilde{g}}$, these branching ratios are of the order of 5% for a 300 GeV gluino and 0.5% for a 1 TeV gluino. There are no other decay modes of the pseudoscalars with considerable branching fractions.

The vector color-octet (**8$_\mathbf{A}$**) gluinonium is not produced by gluon fusion at tree level and does not decay to gluons because the sum of diagrams A, Ã and A' vanishes at threshold.

---

[1]The rate (3.13) is 8 times smaller than that found by [1] which was used in [4–6]. The expression of [7] is the correct one, as can be seen by comparing the **1** and **8$_\mathbf{S}$** cases. For $\mathbf{1} \to gg$, diagrams A and Ã from figure 3 include the color factor

$$\frac{1}{\sqrt{8}}\delta_{ab}f_{age}f_{ehb} = -\frac{3}{\sqrt{8}}\delta_{gh}$$

where g and h are the adjoint indices of the gluons, while $\mathbf{8_S} \to gg$ has the color factor

$$\sqrt{\frac{3}{5}}d_{abc}f_{age}f_{ehb} = -\sqrt{\frac{3}{5}}\left(d_{gac}f_{bea} + d_{gba}f_{cea}\right)f_{ehb} = -\sqrt{\frac{3}{5}}\frac{3}{2}d_{ghc}$$

Squaring and summing over g and h, we obtain $\Gamma_{\mathbf{1}\to gg}/\Gamma_{\mathbf{8_S}\to gg} = 4\left|\psi_\mathbf{1}(\mathbf{0})\right|^2/\left|\psi_\mathbf{8_S}(\mathbf{0})\right|^2$, as in [7]. The mistake of [1] is that they summed over the color index c of the decaying gluinonium in their (2.10).
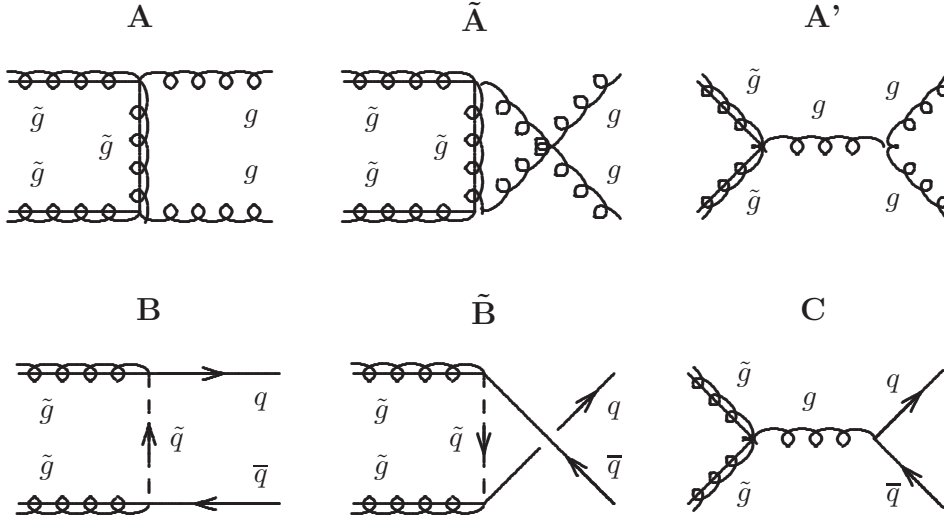
Figure 3. Diagrams for annihilation decays of gluinonia.

It annihilates into $q\overline{q}$ pairs via diagrams B, $\tilde{\text{B}}$ and C in figure 3. The rate is (based on [7] and the $m_{\tilde{q}}$-dependent prefactor taken from, e.g., the calculation of [32] for $q\overline{q} \to \tilde{g}\tilde{g}$)

$$\Gamma(\mathbf{8_A} \to q\overline{q}) = \sum_{\tilde{q}} \left(\frac{m_{\tilde{q}}^2 - m_{\tilde{g}}^2}{m_{\tilde{q}}^2 + m_{\tilde{g}}^2} \right)^2 \frac{\pi \alpha_s^2}{2m_{\tilde{g}}^2} |\psi_{\mathbf{8_A}}(\mathbf{0})|^2 = \sum_{\tilde{q}} \left(\frac{m_{\tilde{q}}^2 - m_{\tilde{g}}^2}{m_{\tilde{q}}^2 + m_{\tilde{g}}^2} \right)^2 \frac{27}{128} \alpha_s^2 \overline{\alpha}_s^3 m_{\tilde{g}} \,, \quad (3.16)$$

where the summation is over the flavors and chiralities of the squarks.

Interestingly, whenever a squark has $m_{\tilde{q}} = m_{\tilde{g}}$ its contribution vanishes because of the destructive interference of diagrams B and $\tilde{\text{B}}$, which depend on the squark masses $m_{\tilde{q}}$, with diagram C, which does not. If the squarks are much heavier than the gluinos, only diagram C contributes, and (3.16) reduces to [7]

$$\Gamma(\mathbf{8_A} \to q\overline{q}) = \frac{27}{64} n_f \alpha_s^2 \overline{\alpha}_s^3 m_{\tilde{g}} \,, \quad (3.17)$$

where n_f is the number of quark flavors.

Numerically, all the annihilation widths are very small, below 1 GeV. Since these decay widths are many orders of magnitude smaller than the gluinonium mass, the gluinonia can effectively be treated as 0-width resonances decaying to dijets and $t\overline{t}$. The annihilation decay modes then have the potential to lead to a precise measurement of the gluino mass. If the decay rates are small enough the colored gluinonia will even hadronize with standard model particles before annihilating. However, since $1/a_0 \gg \Lambda_{\text{QCD}}$, the gluinonium within the hadron will be much smaller than the hadron itself, and so the annihilation decays are insensitive to whether or not the gluinonia are confined.

As expected from (3.1), in cases when the gluinonium decays primarily by annihilation ($\Gamma^{\text{ann}} \gg 2\Gamma_{\tilde{g}}$), its width is much smaller than the binding energy. In fact, for the three

bound states,

$$\frac{1}{E_b}\Gamma^{\mathrm{ann}}(\mathbf{1}, \mathbf{8_S}, \mathbf{8_A}) \sim \alpha_s^2 \overline{\alpha}_s \left(27, \frac{27}{8}, \frac{3}{4}n_f \right) \sim (0.03, 0.003, 0.004) \,. \qquad (3.18)$$

Such gluinonia will appear as distinct states separated from the gluino pair continuum. This also provides a self-consistency check on our use of the narrow width approximation instead of the full NRQCD formalism which we needed for toponium.

3.3 Cross sections at the LHC

As we observed, annihilation decays dominate over other gluinonia decay modes when the squarks are all at least as heavy as the gluino. This is of course possible in parts of the MSSM, since all the superpartner masses are free parameters. To see whether this parameter region corresponds to any viable models motivated by other considerations, we list in table 1 the relevant parameters for a standard set of MSSM benchmark points, the SPS points [10]. In many of these scenarios $2\Gamma_{\tilde{g}} \gg \Gamma^{\mathrm{ann}}$ so the gluinos will decay much more than annihilate, or, if $2\Gamma_{\tilde{g}} \gtrsim E_b$, they will even decay before forming bound states, reducing the situation to one similar to toponium. These decays will contribute to the usual single-gluino decay signature as in the continuum gluino-pair production and the size of this contribution has been studied recently in [8]. We are interested in cases where $2\Gamma_{\tilde{g}} \lesssim \Gamma^{\mathrm{ann}} \ll E_b$ since this is when there is a chance to see the annihilation decays. For the pseudoscalar gluinonia ($\mathbf{1}$ and $\mathbf{8_S}$) the rate for annihilation decays is significant for the SPS 2 (mSUGRA focus point) and SPS 8 (GMSB with neutralino NLSP) scenarios. In these models, two body decays of the gluino are forbidden. For the other SPS points, the gluino decays too fast for annihilation decays to be relevant. The annihilation rate of the vector gluinonium ($\mathbf{8_A}$) turns out to typically have a sizeable suppression due to the $m_{\tilde{q}}$-dependent factor in (3.16), as also shown in table 1. Nevertheless, its annihilation is still significant at SPS 2. We can conclude that there are models in which annihilation decays may be observable. Since including the effect of a finite branching ratio is trivial, in our simulations we will assume $\Gamma_{\tilde{g}} = 0$. It is this limit that is indicated by the last rows in table 1. We consider two representative cases: all the squarks degenerate with the gluinos (which is roughly the case in most of the SPS points) and all the squarks much heavier than the gluinos (like in split SUSY).

In the narrow width approximation, the production cross sections for gluinonia are simply related to their decays through (B.8):

$$\hat{\sigma}_{gg \to \mathbf{1}}(\hat{s}) \simeq \frac{\pi^2 \, \Gamma_{\mathbf{1} \to gg}}{8M_{\mathbf{1}}} \delta\left(\hat{s} - M_{\mathbf{1}}^2 \right) \simeq \frac{243\pi^2}{64} \alpha_s^2 \overline{\alpha}_s^3 \, \delta\left(\hat{s} - M^2 \right) \,,$$

$$\hat{\sigma}_{gg \to \mathbf{8_S}}(\hat{s}) \simeq \frac{\pi^2 \, \Gamma_{\mathbf{8_S} \to gg}}{M_{\mathbf{8_S}}} \delta\left(\hat{s} - M_{\mathbf{8_S}}^2 \right) \simeq \frac{243\pi^2}{256} \alpha_s^2 \overline{\alpha}_s^3 \, \delta\left(\hat{s} - M^2 \right) \,,$$

$$\hat{\sigma}_{q_i \overline{q}_i \to \mathbf{8_A}}(\hat{s}) \simeq \frac{32\pi^2 \, \Gamma_{\mathbf{8_A} \to q_i \overline{q}_i}}{3M_{\mathbf{8_S}}} \delta\left(\hat{s} - M_{\mathbf{8_A}}^2 \right)$$

$$\simeq \frac{9\pi^2}{8} \sum_{\chi=1,2} \left(\frac{m_{\tilde{q}_{i,\chi}}^2 - m_{\tilde{g}}^2}{m_{\tilde{q}_{i,\chi}}^2 + m_{\tilde{g}}^2} \right)^2 \alpha_s^2 \overline{\alpha}_s^3 \, \delta\left(\hat{s} - M^2 \right) \,, \qquad (3.19)$$

– 12 –

Model	$m_{\tilde{g}}$	$m_{\tilde{t}}$	$E_b^{\mathbf{1}}$	$E_b^{\mathbf{8}}$	$2\,\Gamma_{\tilde{g}}$	$\Gamma_{\mathbf{1}}^{\mathrm{ann}}$	$\Gamma_{\mathbf{8_S}}^{\mathrm{ann}}$	$\left(\Gamma_{\mathbf{8_A}}^{\mathrm{ann}}\right)$	$\Gamma_{\mathbf{8_A}}^{\mathrm{ann}}$	σ^{cont}	σ^{bound}	$\sigma_{jj}^{\mathrm{ann}}$	$\sigma_{t\bar{t}}^{\mathrm{ann}}$
	GeV	GeV	GeV	GeV	GeV	MeV	MeV	MeV	MeV	pb	fb	fb	fb
SPS 1a	607	400	18	5.3	11	460	18	25	0.5	6.3	240	7.2	0.14
SPS 1b	938	660	25	7.4	20	530	21	29	0.6	0.30	13	0.3	0.00
SPS 2	782	950	22	6.5	0.0052	500	20	27	8.2	1.7	51	46	0.41
SPS 3	935	648	25	7.4	23	530	21	29	0.6	0.34	13	0.2	0.00
SPS 4	733	545	21	6.1	4.2	490	19	26	0.3	1.8	70	5.5	0.06
SPS 5	722	262	20	6.1	23	490	19	26	1.6	2.4	77	1.2	0.02
SPS 6	720	503	20	6.1	11	490	19	26	0.5	2.0	79	2.5	0.03
SPS 7	950	807	25	7.5	8.4	530	21	29	0.2	0.30	12	0.5	0.00
SPS 8	839	978	23	6.8	0.034	510	20	27	1.7	0.81	28	22	0.10
SPS 9	1182	930	30	8.8	9.1	570	23	31	0.3	0.027	2.2	0.1	0.00
Toy models	300	300	11	3.1	0	370	15	19	0	500	14000	13000	780
	300	∞	11	3.1	0	350	14	19	19	900	15000	15000	240
	800	800	22	6.6	0	500	20	27	0	1.6	39	38	0.28
	800	∞	22	6.6	0	500	20	27	27	3.8	54	51	2.6

Table 1. Parameters of various standard MSSM points and the toy scenarios that we will analyze. The column $\left(\Gamma_{\mathbf{8_A}}^{\mathrm{ann}}\right)$ refers to the value without the $m_{\tilde{q}}$-dependent suppression factor in (3.16). We also compare the gluinonia production cross section σ^{bound} (estimated in the narrow-width approximation) with the continuum gluino-pair production cross section σ^{cont}, and the last two columns show the annihilation cross sections into dijets and $t\bar{t}$ (while the rest of σ^{bound} corresponds to single gluino decays like in the continuum).

where the sum in the last line is over squark chiralities.

Alternatively, the expressions for the cross section can be derived using the near-threshold tree-level gluino pair production cross sections, which are (see, e.g., [32])

$$\frac{\hat{\sigma}_0(gg \to \tilde{g}\tilde{g})}{\beta} = \frac{27\pi\alpha_s^2}{64 m_{\tilde{g}}^2}, \qquad \frac{\hat{\sigma}_0(q_i\overline{q}_i \to \tilde{g}\tilde{g})}{\beta} = \frac{\pi\alpha_s^2}{6m_{\tilde{g}}^2} \sum_{\chi=1,2} \left(\frac{m_{\tilde{q}_{i,\chi}}^2 - m_{\tilde{g}}^2}{m_{\tilde{q}_{i,\chi}}^2 + m_{\tilde{g}}^2}\right)^2 . \quad (3.20)$$

In the gg channel $1/6$ of the production is in the color-singlet representation, $1/3$ in the color-octet $\mathbf{8_S}$, and $1/2$ in $\mathbf{27}$ (which does not bind), while in the $q\overline{q}$ channel all the production is in the color-octet $\mathbf{8_A}$ [8]. Then, using eq. (A.10) from appendix A, with the wavefunctions in eq. (3.7) computed with the color factors of eq. (3.9) appropriate for each representation, we obtain eq. (3.19).

The radial excitations are described by the same expressions as (3.19), but with the annihilation widths scaled by

$$\Gamma^{\mathrm{ann}} \to \frac{\Gamma^{\mathrm{ann}}}{n^3} . \quad (3.21)$$

In the limit $\Gamma_{\tilde{g}} \to 0$ the radial excitations can be summed to effectively change Γ^{ann} by an overall prefactor

$$\sum_{n=1}^{\infty} \frac{1}{n^3} = \zeta(3) \simeq 1.202 . \quad (3.22)$$

$m_{\tilde{g}}$	$m_{\tilde{q}}$	$\mathbf{1}, \mathbf{8_S} \to gg$	$\mathbf{1}, \mathbf{8_S} \to t\bar{t}$	$\mathbf{8_A} \to q\bar{q}$	$\mathbf{8_A} \to t\bar{t}$	any $\to gg, q\bar{q}$	any $\to t\bar{t}$
GeV	GeV	fb	fb	fb	fb	fb	fb
300	300	13000	780	0	0	13000	780
300	∞	14000	0	1200	240	15000	240
800	800	38	0.28	0	0	38	0.28
800	∞	38	0	13	2.6	51	2.6

Table 2. Gluinonium annihilation cross sections at the LHC.

For a finite $\Gamma_{\tilde{g}}$ the contribution of the radial excitations is somewhat smaller.[2]

The total production cross sections are given by

$$\sigma(pp \to \mathbf{1}) = \zeta(3) \frac{\pi^2}{8M_{\mathbf{1}}^3} \mathcal{L}_{gg}(M_{\mathbf{1}}^2) \, \Gamma_{\mathbf{1} \to gg} \,, \tag{3.23}$$

$$\sigma(pp \to \mathbf{8_S}) = \zeta(3) \frac{\pi^2}{M_{\mathbf{8_S}}^3} \mathcal{L}_{gg}(M_{\mathbf{8_S}}^2) \, \Gamma_{\mathbf{8_S} \to gg} \,, \tag{3.24}$$

$$\sigma(pp \to \mathbf{8_A}) = \zeta(3) \frac{64\pi^2}{3M_{\mathbf{8_A}}^3} \sum_q \mathcal{L}_{q\bar{q}}(M_{\mathbf{8_A}}^2) \, \Gamma_{\mathbf{8_A} \to q\bar{q}} \,, \tag{3.25}$$

where the luminosities are

$$\mathcal{L}_{ij}(\hat{s}) = \frac{\hat{s}}{s} \int_{\hat{s}/s}^1 \frac{\mathrm{d}x}{x} \, f_i(x) \, f_j\left(\frac{\hat{s}}{xs}\right) \,, \tag{3.26}$$

where i and j denote the initial state partons and $\sqrt{s} = E_{\mathrm{CM}}$ is the collider energy.

These cross sections are shown in figure 4 as a function of the gluinonium mass for the LHC at $\sqrt{s} = 14\,\mathrm{TeV}$, $10\,\mathrm{TeV}$ and $7\,\mathrm{TeV}$. For this plot, we have used the LO MSTW 2008 parton distribution functions [33] evaluated at the scale $M = 2m_{\tilde{g}}$ and neglected both the gluino width $\Gamma_{\tilde{g}}$ and the suppression of $\Gamma_{\mathbf{8_A} \to q\bar{q}}$ due to the finite squark masses. These cross sections sum to a few percent of the total gluino pair production cross section, fairly independently of the gluino mass over this range. We will discuss this further in section 6.1.

The cross sections for sample masses $m_{\tilde{g}} = 300$ and $800\,\mathrm{GeV}$, with squarks either degenerate with the gluinos or much heavier, are shown in table 2. These numbers differ somewhat from other results in the literature. Ref. [7] has found cross sections which are a factor of $2 - 3$ smaller than our results. This happens to a large extent because they use α_s^3 instead of $\overline{\alpha}_s^3$ in their expressions for $|\psi(\mathbf{0})|^2$. The results of [4] for the pseudoscalar gluinonium are about 4 times bigger than ours (even though they applied certain cuts while we did not). Because of the factor-of-8 error in the expression they use for $\Gamma_{\mathbf{8_S} \to gg}$ as we explained in Footnote 1, their combined cross section for $\mathbf{1}$ and $\mathbf{8_S}$ is indeed expected to

---

[2]For finite $\Gamma_{\tilde{g}}$, the excited modes, with their $1/n^3$-reduced annihilation rate, still need to compete with the same $2\Gamma_{\tilde{g}}$. The correct correction can be easily computed numerically. One can also take into account that some of the excited states may decay into P states whose annihilation rates are small. This reduces their contribution to the annihilation signal. We do not take this possibility into account. We also did not take into account the direct production of P states and higher angular excitations.
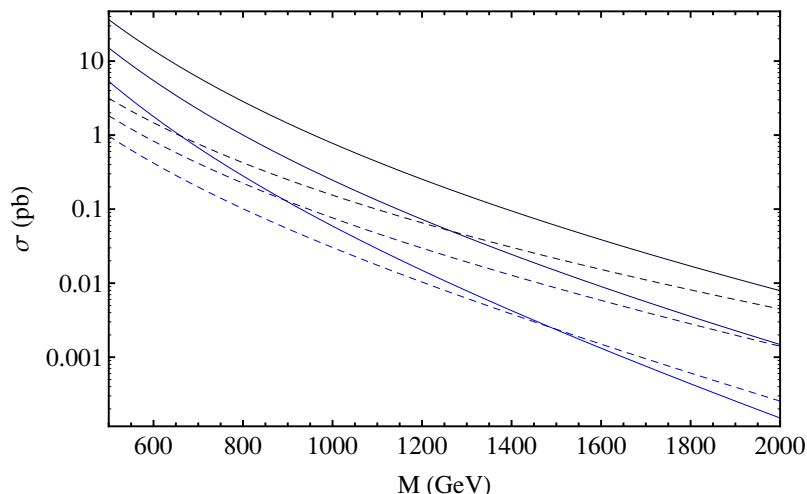
Figure 4. Gluinonia production cross section at the LHC as a function of the gluinonium mass $M \simeq 2m_{\tilde{g}}$. Solid lines refer to the sum of **1** and **8$_\mathbf{S}$** pseudoscalar gluinonia which annihilate into gg and $t\bar{t}$, and dashed lines refer to **8$_\mathbf{A}$** vector gluinonium which annihilates into $q\bar{q}$ (including $t\bar{t}$). The three lines in each case correspond, from top to bottom, to LHC center-of-mass energy of $\sqrt{s} = 14$, 10 and 7 TeV.

be by a factor of about 2.4 larger. However, it also seems that they used α_s instead of $\overline{\alpha}_s$, which should have made their result smaller. But they have included a K-factor of 2.0 which can compensate for that. A K-factor does need to be included in principle, but its size is still unknown. The effect of initial-state radiation on the gluinonium production has been computed in [8], giving a near-threshold K-factor that varies from 1.2 for $m_{\tilde{g}} = 200\,\text{GeV}$ to 1.8 for $m_{\tilde{g}} = 1\,\text{TeV}$. However, this does not yet include the emission of non-collinear gluons which can give an additional correction of the same order [8]. Other corrections which can modify the results by $\sim 50\%$ are higher-order QCD corrections to the potential (2.1), a confining term that may still affect the result for the smaller masses, and relativistic corrections suppressed by v^2. Computations of part of the QCD corrections have been recently presented in [9]. Furthermore, we need to include corrections also to the annihilation process (final-state radiation etc.). Since some of these quantities have not been computed yet, we will not include a K-factor in our simulation of the gluinonium signal. We will not include a K-factor for the QCD background either.

4   Gluinonium: simulation

In the previous section, we found that $300\,\text{GeV}$ gluinos can have a cross section for annihilation decay as high as 15 pb. Although the cross sections shrink sharply with gluino mass, it is certainly possible that the annihilation decays of gluinonia might be seen. The dominant decay mode of the gluinonia is to dijets, however the decays to $t\bar{t}$ may be easier to see because of smaller backgrounds. In order to determine what we might learn about

the underlying physics if these resonances can be found, we now examine the dijet and $t\bar{t}$ signals and backgrounds through Monte Carlo simulation.

We simulate both the signals and backgrounds at the LHC at 14 TeV using PYTHIA version 8.120 [34–36] with MSTW2008 LO parton distribution functions [33]. For clustering the particles into jets, we use the SISCONE jet algorithm version 2.0.1 [37, 38] with radius $R = 1$ for the dijet analyzes and $R = 0.5$ for the $t\bar{t}$ analysis.

4.1 Signal and background

As we saw in the previous section, the bound states of different spin have different production and decay modes. The pseudoscalars, which include a color-singlet, $\Phi_{\mathbf{1}}$, and a color-octet, $\Phi_{\mathbf{8_S}}$, couple to both gluons and heavy quarks. In models for which the annihilation decays are relevant, the resonances have very small widths. Then we can model them with effective interactions of the form

$$\mathcal{L}_{\mathbf{1}} = c_{gg}^{\mathbf{1}} \frac{1}{m_{\tilde{g}}} \epsilon^{\mu\nu\rho\sigma} \Phi_{\mathbf{1}} G_{\mu\nu}^{a} G_{\rho\sigma}^{a} + c_{q\bar{q}}^{\mathbf{1}} \frac{m_q}{m_{\tilde{g}}} \Phi_{\mathbf{1}} \, i\bar{q}\gamma^5 q \,, \tag{4.1}$$

$$\mathcal{L}_{\mathbf{8_S}} = c_{gg}^{\mathbf{8_S}} \frac{1}{m_{\tilde{g}}} \epsilon^{\mu\nu\rho\sigma} d^{abc} \Phi_{\mathbf{8_S}}^{a} G_{\mu\nu}^{b} G_{\rho\sigma}^{c} + c_{q\bar{q}}^{\mathbf{8_S}} \frac{m_q}{m_{\tilde{g}}} \Phi_{\mathbf{8_S}}^{a} (T^a)_i^j \, i\bar{q}^i\gamma^5 q_j \,, \tag{4.2}$$

where a, b, c and i, j are color indices of the adjoint and fundamental representations, respectively. The factor of m_q in the normalization of the $q\bar{q}$ operators is chosen so that they vanish as $m_q \to 0$, as they must by chirality (the rates are approximately proportional to m_q^2: see (3.14) and (3.15)). The vector, $V_{\mathbf{8_A}}^{\mu}$, has suppressed couplings to gluons and its coupling to quarks can be described by the effective interaction

$$\mathcal{L}_{\mathbf{8_A}} = c_{q\bar{q}}^{\mathbf{8_A}} \left(V_{\mathbf{8_A}}^{\mu} \right)^a (T^a)_i^j \, \bar{q}^i\gamma_\mu q_j \,. \tag{4.3}$$

All of the coefficients $c_{gg}^{\mathbf{R}}$ and $c_{q\bar{q}}^{\mathbf{R}}$ are fixed by matching to the annihilation rates. One could also write down operators with additional derivatives, but since in the narrow width approximation the momenta of the incoming particles are fixed, we can simply absorb the effect of these additional operators into the normalization.

As a simplifying assumption, since the color matrices do not affect the geometry of the processes, at least at leading order, we treat all the gluinonia as color-singlets. This facilitates the Monte Carlo simulation. In particular, the pseudoscalar gluinonia reduce to a pseudoscalar Higgs with appropriately modified couplings. The vector gluinonium can be simulated as a vector Z' with flavor universal couplings of appropriate strength (to the vector current of quarks only). We restrict our discussion of the simulation results to the representative cases described in table 2, with $m_{\tilde{g}} = 300\,\text{GeV}$ ($M = 600\,\text{GeV}$) and $m_{\tilde{g}} = 800\,\text{GeV}$ ($M = 1600\,\text{GeV}$).

The background for the dijet signals (gg and $q\bar{q}$) is QCD dijets. For the $t\bar{t}$ channel background, we use the standard model $t\bar{t}$ production, including both $gg \to t\bar{t}$ ($\sim 85\%$) and $q\bar{q} \to t\bar{t}$ ($\sim 15\%$) and also single top production (predominantly $qq \to tq$). We do not include fakes from QCD or $W/Z + \text{jets}$ since it seems likely the experiments can distinguish these backgrounds from $t\bar{t}$ with good efficiency [39], but in any case, top-tagging is a subject largely orthogonal to the current work.
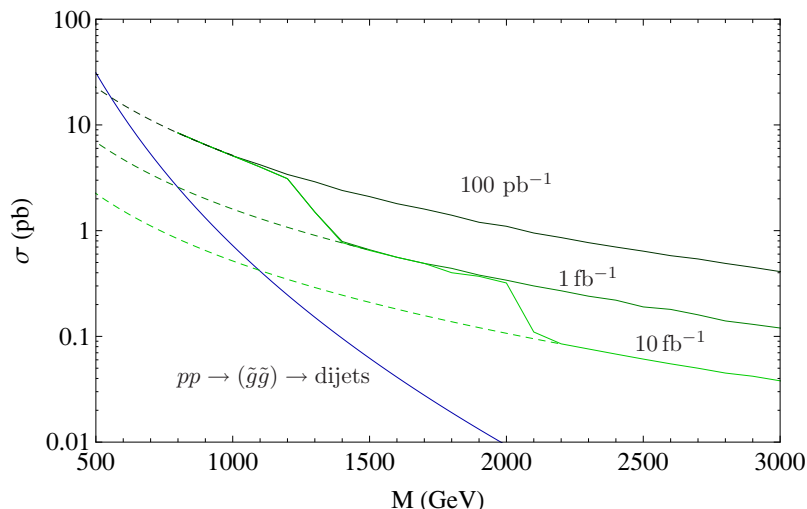
Figure 5. Dijet search reach (95% confidence level exclusion) at CMS [40] and the gluinonium signal with $|\eta_{\rm jet}| < 1$. The steps are due to prescaling. The dashed lines are our extrapolations assuming that the prescaling can be reduced by adjusting the triggers.

4.2 Analysis of the dijet channel

First, let us consider the dijet signatures of annihilation decays. These come from pseudoscalars decaying to gg and vectors decaying to $q\bar{q}$. For the $m_{\tilde{g}} = 300\,{\rm GeV}$ case, the jets will dominantly have $p_T \gtrsim 200\,{\rm GeV}$, and for the $m_{\tilde{g}} = 800\,{\rm GeV}$ case $p_T \gtrsim 500\,{\rm GeV}$. For the light gluino, the $200\,{\rm GeV}$ p_T cut is problematic because it will not survive the high-luminosity triggers of either ATLAS or CMS. For example, with an instantaneous luminosity of $10^{34}\ {\rm cm}^{-2}\ {\rm s}^{-1}$, only dijet events with $p_T > 450\,{\rm GeV}$ can survive prescaling. As pointed out in [40], if we already have information about the gluino mass, for example from cascade decays, than the high-level trigger can be adjusted to reduce the prescaling by a factor of up to 1000. Therefore, it is still possible that the dijet signatures of the $600\,{\rm GeV}$ gluinonium annihilation decays may be found. In figure 5, we compare the dijet reach at CMS (for instantaneous luminosities of 10^{32}, 10^{33} and $10^{34}\ {\rm cm}^{-2}\ {\rm s}^{-1}$) to the gluinonium cross section. The sawtooth shape of the reach is due to prescaling, so we have extrapolated these curves to lower mass, assuming the prescaling can be overcome by adjusting the high-level trigger.

To study the distributions, we simulate the signals and the backgrounds requiring two jets with $p_T > 200\,{\rm GeV}$ for the $m_{\tilde{g}} = 300\,{\rm GeV}$ case and two jets with $p_T > 500\,{\rm GeV}$ for the $m_{\tilde{g}} = 800\,{\rm GeV}$ case. Figure 6 shows the distribution of the invariant mass of the two hardest jets in these samples. Note that the signal, whose intrinsic width is a fraction of a GeV, broadens to about 5% of the mass of the resonance due to QCD radiation (the scaling of the radiation width with the mass of the resonance follows by dimensional analysis, since QCD is almost conformal at these energies). The enormous background and trigger issues (for the light gluino case) notwithstanding, the gluino mass can, in principle, be determined from the location of dijet invariant mass peak.

Let us now study more closely the behavior of the signal and the background near the peak, in the window of $580\,{\rm GeV} < M_{jj} < 620\,{\rm GeV}$ for $m_{\tilde{g}} = 300\,{\rm GeV}$ and $1560\,{\rm GeV} <$
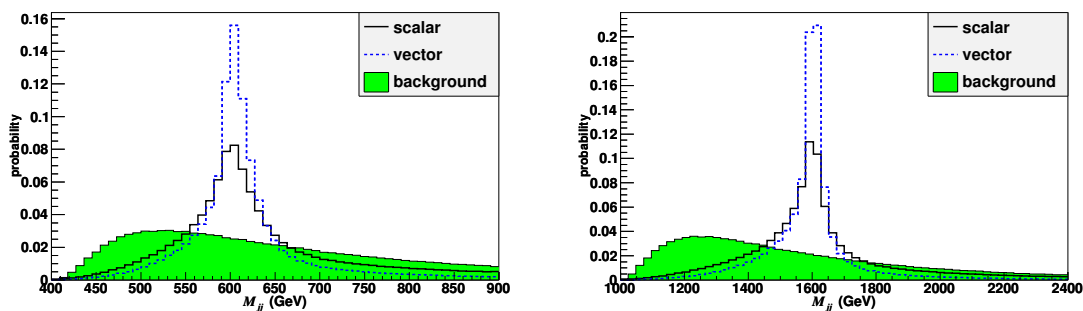
Figure 6. The invariant mass of the two hardest jets. Left is the 300 GeV gluino and background after a $p_T^{\text{jet}} > 200$ GeV cut, and right is the 800 GeV gluino and background with a $p_T^{\text{jet}} > 500$ GeV cut.
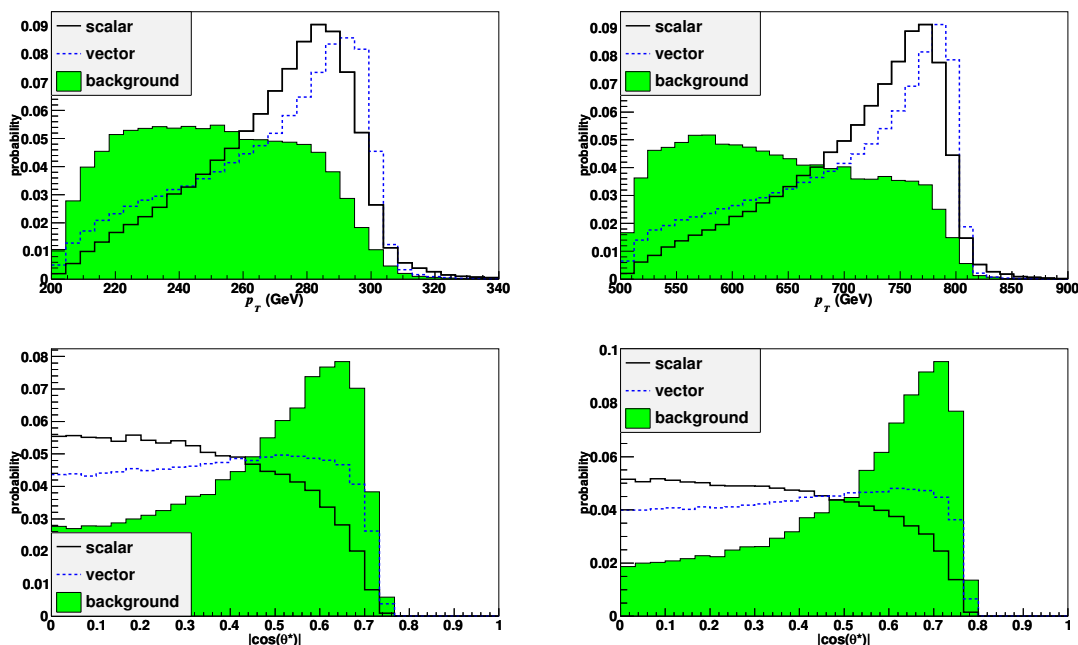

Figure 7. Distributions of the average transverse momentum of the two hardest jets (top row) and the scattering angle in the collision frame (bottom row), in invariant mass range 580 GeV < M_{jj} < 620 GeV for the 300 GeV gluino case (left) and in invariant mass range 1560 GeV < M_{jj} < 1640 GeV for the 800 GeV gluino (right).

M_{jj} < 1640 GeV for $m_{\tilde{g}} = 800$ GeV. In figure 7, we show the distributions of p_T and the scattering angle $\cos\theta^\star$. As expected and can be seen from these plots, the angular distribution is sensitive to the spin of the resonance. In principle, this information can be used to verify that the resonance is indeed the gluinonium. The experiment will measure the sum of contributions from two different spins, but as can be seen from table 2 or figure 4, the spin-0 contribution will typically dominate.

To explore the signal and background rates more quantitatively, consider the 300 GeV gluino. In the dijet invariant mass window 580 GeV < M_{jj} < 620 GeV, including both the

spin-0 and spin-1 resonance contributions, the signal-to-background ratio is $S/B \simeq 1 \times 10^{-3}$ after the cuts $p_T > 275\,\text{GeV}$, $|\cos\theta^\star| < 0.5$ for both cases from table 2. This indicates that the signal extraction will be very sensitive to theoretical and experimental systematic uncertainties of the background. On the other hand, the statistical uncertainty on the background, characterized by $S/\sqrt{B}$, quickly shrinks because we are dealing with a large number of events. For example, with $\sim 10\,\text{fb}^{-1}$ there is already a 3σ significance. Although the CMS analysis [40] indicates that these signals may be seen (see figure 5),[3] enhancing the signal-to-background ratio may be critical to getting a clean sample from which the gluinonium spin might be extracted. Possibilities for enhancing the signal might involve jet substructure [41], color information, additional angular variables, or multivariate techniques. These ideas are worth pursuing, but go beyond the scope of the current paper. No matter what, detecting and characterizing the dijet annihilation decay signal of gluinonium will be a formidable challenge.

4.3 Analysis of the $t\bar{t}$ channel

Another possible decay mode of gluinonium is to $t\bar{t}$. As we have shown, this decay rate depends on the masses of the squarks as well as the gluino mass. For a 300 GeV gluino and 300 GeV squarks, the cross section times branching ratio to $t\bar{t}$ is 780 fb. If the squarks are decoupled, the cross section is reduced to 240 fb. Although these cross sections are small, the systematic uncertainty on the $t\bar{t}$ background is much smaller than for dijets, so there is hope that with enough integrated luminosity, such resonances may be seen. There has also been a fair amount of recent progress in improving the techniques to find boosted tops [42–45], which would come from very heavy gluinonium decays.

The reconstruction of the invariant mass and the other properties of the decaying resonance in the $t\bar{t}$ channel is more complicated than in the dijet case because the tops decay. As a result, the energy and momentum of the resonances are no longer concentrated in two hard jets, but in a combination of several jets and possibly leptons and missing energy as well. The cleanest channel for $t\bar{t}$ is the semi-leptonic one, in which one of the tops decays hadronically and the other decays to a b-quark, an electron or muon, and a neutrino. The presence of the lepton (unlike in the all-hadronic channel) is very useful for rejecting the QCD background, while the fact that there is only a single neutrino (unlike in the all-leptonic channel) allows full reconstruction using the on-shell intermediate W. The branching ratio for semi-leptonic $t\bar{t}$ is 30%, and, for simplicity, we consider only this channel. The top-tagging algorithm we use is described in appendix C.

The resulting $t\bar{t}$ invariant mass peak is fairly sharp, as shown in figure 8. To study the signal in more detail we now restrict to the mass window $575\,\text{GeV} < M_{t\bar{t}} < 625\,\text{GeV}$. The p_T and $\cos\theta^\star$ distributions in this window are shown in figure 9. The difference between the angular distributions of the scalar and the vector is much smaller here than in the dijet case because the top is not much lighter than the 300 GeV gluino. In the limit of very

---

[3]Note however that while the analysis in [40] has taken into account the statistical noise of the background, the resolution limitations, and the various systematic uncertainties, it has not simulated the subtraction of the background from the data, which we guess is likely to be a critical issue with the small S/B that we have.
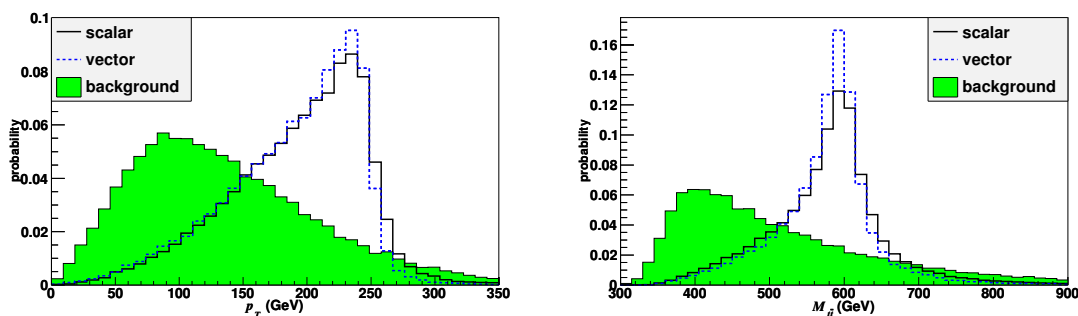
Figure 8. Distributions of the average p_T (left) and invariant mass (right) of the $t\bar{t}$ pair for a 300 GeV gluino.
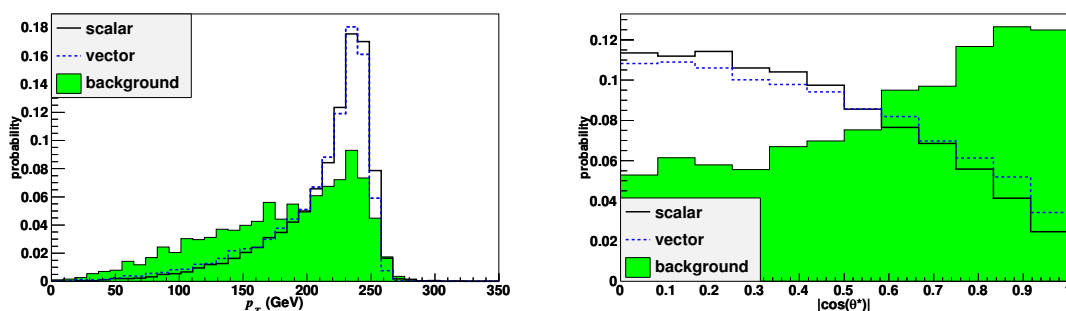

Figure 9. Distributions of the average p_T (left) and the scattering angle of the $t\bar{t}$ pair in the collision frame (right) for the 300 GeV gluino in invariant mass range 575 GeV $< M_{t\bar{t}} <$ 625 GeV.

heavy gluinonium, the differences between the spins reappear, but the cross section for the $t\bar{t}$ signal drops too fast to make this channel useful (from table 2, for $m_{\tilde{g}} = 800$ GeV, $\sigma_{t\bar{t}} \sim 3$ fb if the squarks are decoupled and an order of magnitude smaller if they are degenerate with the gluinos).

For the case $m_{\tilde{g}} = m_{\tilde{q}} = 300$ GeV we obtain $S/B = 1.6 \times 10^{-2}$ and $S/\sqrt{B} = 3$ at 500 fb^{-1} after applying the cuts $p_T > 200$ GeV, $|\cos\theta^\star| < 0.5$. These estimates are somewhat less promising than what has been found in generic analysis of resonances decaying into $t\bar{t}$ by ATLAS [46]. For example, they find that 300 fb^{-1} of luminosity will allow a 5σ discovery of a 600 GeV resonance if its cross section is above ~ 700 fb, which is approximately the cross section we have. In contrast to the dijet channel, the $t\bar{t}$ search is entirely statistics limited. The reach could be improved somewhat by inclusion of other $t\bar{t}$ decay channels, and through an optimization of the cuts and top-tagging algorithm. We conclude that $t\bar{t}$ is a viable, but high luminosity, channel in which gluinonium, if it exists, could almost certainly eventually be found.

4.4 Estimate for the diphoton channel

Since the gluinos are not charged under the electroweak group, the gluinonia can decay into electroweak bosons such as $\gamma\gamma$ only through loops, with branching fractions of $\sim 10^{-5}$ [9]. Nevertheless, it might still be useful to consider the diphoton channel because of its much

smaller background compared to the dijet and $t\bar{t}$ channels. We have not performed a complete analysis, but it is easy to get a rough idea by comparing to the analysis of the $\gamma\gamma$ signal of the squarkonium in [47] which we will mention in the next section. It turns out that the small $\gamma\gamma$ branching ratio for the gluinonium compared to the squarkonium is roughly compensated by the larger color factors in the gluinonium production process, and the signal may be observable if the gluino is relatively light.[4] For $m_{\tilde{g}} \sim 300\,\mathrm{GeV}$, we will have S/B of about 10%, which is much better than in the dijet or $t\bar{t}$ channel, but 3σ significance will require almost $10^3\,\mathrm{fb}^{-1}$ of luminosity.

5 Squarkonium and other QCD bound states

So far we discussed the bound states of color-fundamental fermions (toponium) and color-adjoint fermions (gluinonium). We have seen that relative to the decay rate of the tops, the annihilation decays of toponium have a too small branching ratio to be detectable. On the other hand, the gluino is sufficiently long-lived in certain regions of parameter space, so gluinonium may have observable decays to dijets and $t\bar{t}$. Let us now discuss the other possible bound states of particles charged under QCD. In the MSSM, the only other colored particles are squarks, which are scalars in the fundamental representation. There exist strong production processes (see for example [32, 48]) for a squark-antisquark pair

$$gg \to \tilde{q}_i\bar{\tilde{q}}_i\,, \qquad q_i\bar{q}_j \to \tilde{q}_k\bar{\tilde{q}}_l\,, \tag{5.1}$$

a pair of squarks

$$q_iq_j \to \tilde{q}_i\tilde{q}_j\,, \tag{5.2}$$

or a squark and a gluino

$$q_ig \to \tilde{q}_i\tilde{g}\,. \tag{5.3}$$

Let us discuss the possible bound states of these particles.

5.1 Squarkonium

Squarkonium is a bound state of a squark and an antisquark. As in the case of toponium, the color decomposes as

$$\mathbf{3} \otimes \overline{\mathbf{3}} = \mathbf{1} \oplus \mathbf{8}\,, \tag{5.4}$$

and only the color singlet can bind. The color factor for the singlet bound state is

$$C_{\mathbf{1}} = \frac{4}{3}\,. \tag{5.5}$$

In most scenarios squarkonia do not form because the squarks decay too fast. For the gluino, we could make the single-particle decay rate arbitrarily small by making all the squarks heavy. However, because squarks have electroweak quantum numbers and are heavier than the lightest supersymmetric particle (LSP), they can generically decay as

$$\tilde{q} \to \tilde{q}'\,W \qquad \text{or} \qquad \tilde{q} \to q\,\chi\,, \tag{5.6}$$

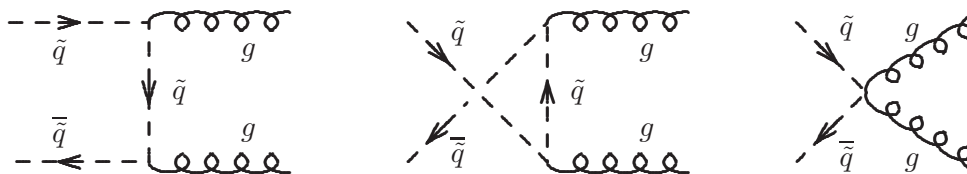[4]We thank Cliff Burgess for suggesting us to check this possibility.

Figure 10. Diagrams for the dominant annihilation decay of stoponium. The first two diagrams do not actually contribute because they vanish at threshold.

Model	$m_{\tilde{t}}$ (GeV)	E_b (GeV)	$2\,\Gamma_{\tilde{t}}$ (GeV)	Γ^{ann} (GeV)
SPS 5 (mSUGRA with light stop)	262	2.3	0.087	0.0028
All other SPS points	≥ 400	~ 5	≥ 3	~ 0.004

Table 3. The mass of the lighter stop $m_{\tilde{t}}$, the binding energy E_b, twice the stop decay rate $2\Gamma_{\tilde{t}}$, and the stoponium annihilation rate Γ^{ann}, for the SPS benchmark points [10]. In all the SPS scenarios, the stop decays roughly equally via $\tilde{t} \to \overline{\chi}^0 t$ and $\tilde{t} \to \overline{\chi}^+ b$ (only the latter is present in SPS 5).

where χ is a chargino or neutralino. The rate for these decays is in general comparable to the binding energy

$$E_b = \frac{4}{9}\overline{\alpha}_s^2 m_{\tilde{q}} \tag{5.7}$$

of the would-be squarkonium and we obtain a situation similar to the toponium in which the bound state is very broad and it decays primarily by single-particle decays rather than the annihilation decays.

The only possible exception is stoponium. There, the stop can be lighter than the top plus LSP, so the weak decays are forbidden. This is not the case in most of the parameter space of the mSUGRA ansatz. In SPS 5, even though the width is smaller than the binding energy, single-stop decays still dominate over the annihilation decays (see table 3). However, the situation is much more favorable in certain other motivated scenarios discussed in more detail in [47, 49].

Stoponium ($J^{\mathrm{PC}} = 0^{++}$) is produced primarily by gluon fusion. Its annihilation into gg via the diagrams in figure 10 has the rate

$$\Gamma(\mathbf{1} \to gg) = \frac{4\pi\alpha_s^2}{3m_{\tilde{q}}^2} \left|\psi(\mathbf{0})\right|^2 = \frac{32}{81}\alpha_s^2\overline{\alpha}_s^3 m_{\tilde{q}}\,. \tag{5.8}$$

Unfortunately, this is about 200 times smaller than for gluinonia of the same mass mostly due to the different color factors (compare to (3.12), and note that in the gluinonium case there are also contributions from the octets), and twice smaller than for a heavy quarkonium of the same mass (see (2.10)), and the production cross section, which is given by (3.23), is correspondingly smaller. As a result, the stoponium cannot be seen in the dijet or $t\overline{t}$ channels even when the annihilation decays dominate.

However, since the squarks are charged, the annihilation of stoponium to $\gamma\gamma$ is relevant. Although the branching ratio to $\gamma\gamma$ is only $\sim (8/9)(\alpha/\alpha_s)^2 \simeq 0.005$, for certain regions of MSSM parameter space the cross section may still be of order 1 fb which makes it possibly observable. Other stoponium decay modes including ZZ and W^+W^- could possibly be visible as well. Stoponium decays have been studied in detail in [47, 50–53] (note that [50, 51] contain certain factor-of-2 errors — see [47, 54, 55]).

5.2 Di-squark and squark-gluino bound states

Instead of a squark and anti-squark, another possible bound state might be two squarks or a squark and a gluino. For di-squarks, the relevant color decomposition is

$$\mathbf{3} \otimes \mathbf{3} = \overline{\mathbf{3}} \oplus \mathbf{6} \tag{5.9}$$

and the color factors are

$$C_{\overline{\mathbf{3}}} = \frac{2}{3}, \qquad C_{\mathbf{6}} = -\frac{1}{3}, \tag{5.10}$$

so the triplet has an attractive potential and can potentially form a bound state. For a squark-gluino pair, the decomposition is

$$\mathbf{3} \otimes \mathbf{8} = \mathbf{3} \oplus \overline{\mathbf{6}} \oplus \mathbf{15} \tag{5.11}$$

and

$$C_{\mathbf{3}} = \frac{3}{2}, \qquad C_{\overline{\mathbf{6}}} = \frac{1}{2}, \qquad C_{\mathbf{15}} = -\frac{1}{2}, \tag{5.12}$$

which means that the potential for the triplet and the sextet is attractive and could potentially support spin-$\frac{1}{2}$ bound states of these two particles.

However, the di-squarks and the squark-gluino bound states suffer from the same problem as the squarkonium, namely the too rapid decays of the squarks. Furthermore, even the special cases in which the lighter stop is sufficiently stable are not available here because, unlike in the case of the stoponium, producing a di-stop or a stop-gluino bound state via (5.2) or (5.3), respectively, would require having top quarks as incoming partons.

5.3 Other QCD bound states

There are many more possible bound states of hypothetical new colored particles. For example, superheavy quarkonia have been studied in [56, 57] and bound states of $SU(2)_L$-doublet color-octet scalars in [58]. It would also be interesting look at bound states of Kaluza-Klein (KK) excitations of quarks and gluons in theories with extra dimensions. For example, Universal Extra Dimension (UED) models have TeV-scale flat extra dimensions with all the standard model fields propagating in the bulk, so they all have massive excitations. For certain regions of parameter space KK quarks can be sufficiently stable to form bound states [59, 60]. Even though the KK particles are color adjoints or fundamentals, like the gluino or squarks we have already considered, the details of the phenomenology will be somewhat different because of the different spins as well as the different range of possibilities for the single-particle lifetimes, and it would be interesting to study this in more detail in a future work. If annihilation decays can be detected at the LHC, one

interesting application would be to try to use them to distinguish extra dimensions from supersymmetry. From figure 7, there is clearly some spin information contained in the dijets from annihilation, but isolating a clean sample to see this effect may be impossible in practice. The size of the cross sections for the different annihilation channels might also be a useful discriminator, when combined with other information.

6 Bound states with new forces

The previous sections have all looked at bound states for which the binding force is the strong force of QCD. We have seen that being charged under the strong force allows particles to be produced with substantial cross sections, and substantial binding and annihilation rates, as high as tens of picobarns. Our discussion of the phenomenology of colored bound states was centered around supersymmetry, in particular, the MSSM, which has new particles but no new forces as compared to the standard model. However, there are plenty of models which do have new forces. Technicolor is an obvious example, but even within supersymmetric models, dynamical supersymmetry breaking often involves something beyond $SU(3) \times SU(2) \times U(1)$. It is certainly possible for there to be a new force, even stronger than QCD, which would lead to quite substantial annihilation decay rates.

Let us suppose there is a new force associated with a new $SU(N)$ gauge group. If the associated strong coupling scale Λ_N is sufficiently large (say $10\,\mathrm{TeV}$), then all the particles produced at the LHC would be confined into $SU(N)$-singlets. This case is not interesting for the present paper, as there is no way to distinguish particles bound by this force from fundamental resonances. Instead, we are interested in a situation in which the LHC will be able to produce particles with mass $m \gg \Lambda_N \gtrsim \Lambda_{\mathrm{QCD}}$. We further assume they are charged under both QCD and $SU(N)$, so that they will also have substantial production rates. Recall that the annihilation rates are proportional to $|\psi(\mathbf{0})|^2 \propto \overline{\alpha}_s^3$. Since these rates scale as the third power of the coupling, the new gauge coupling does not have to be much larger than the QCD coupling to drastically increase the rate.

To distinguish annihilation decays from simple resonances, we also need to have some other way to observe these new particles. For example, this may be through single particle decays, as with the gluino. In fact, there are many models in which weird things happen when there are new forces, such as displaced vertices in hidden valley models [61], or macroscopic strings in quirks [62]. We will focus only on annihilation decays, leaving their coordination with the rich field of new-force model signatures for future consideration.

6.1 Increasing the annihilation rate

For gluinos of phenomenologically relevant masses, we saw that as the gluino becomes more stable the gluinonium annihilation cross section saturates at a few percent of the continuum gluino pair production cross section. Let us discuss which factors set the scale for this number and what can make it larger, and then consider the situation in which the binding particles have an additional attractive force, beyond the SU(3) of QCD.

The bound state production cross section is given by

$$\sigma^{\text{bound}} \simeq \frac{\mathcal{L}(4m^2)}{m} \int \hat{\sigma}^{\text{bound}}(\hat{s}) \, \mathrm{d}\sqrt{\hat{s}} \sim \frac{\mathcal{L}(4m^2)}{m} \frac{\alpha_s^2}{m^4} |\psi(\mathbf{0})|^2 \sim \mathcal{L}(4m^2) \frac{\alpha_s^2 C^3 \overline{\alpha}_s^3}{m^2}, \quad (6.1)$$

where $\mathcal{L}(M^2)$ is the parton luminosity, eq. (3.26). If we neglect the dependence of the parton luminosities on the energy, then the parton-level continuum production cross section $\hat{\sigma}^{\text{cont}}(\hat{s}) \sim \alpha_s^2/\hat{s}$ gives

$$\sigma^{\text{cont}} \sim \frac{\mathcal{L}(4m^2)}{m} \int \hat{\sigma}^{\text{cont}}(\hat{s}) \, \mathrm{d}\sqrt{\hat{s}} \sim \mathcal{L}(4m^2) \frac{\alpha_s^2}{m^2}, \quad (6.2)$$

so that

$$\frac{\sigma^{\text{bound}}}{\sigma^{\text{cont}}} \sim C^3 \overline{\alpha}_s^3. \quad (6.3)$$

There are additional factors coming from the fact that only part of the color configurations bind, and the fall off of the parton luminosities with energy, but this qualitative scaling still holds. The point is that because C and $\overline{\alpha}_s$ are raised to the third power in this relation, the fraction of annihilation decays can be significantly enhanced over the continuum if the coupling or color factors are larger than they are for QCD.

It is interesting to also consider how large the fraction of annihilation decays can be, while the binding force is still perturbative. When the coupling $\overline{\alpha}_s$ is increased, it not only increases the binding rate, but also adds a radiative correction to the continuum production. This can lead to a significant Sommerfeld enhancement of the total cross section. From eq. (A.13), the additive correction to the continuum production near the threshold is roughly

$$\Delta\hat{\sigma}^{\text{cont}}(\hat{s}) \sim \frac{\alpha_s^2}{m^2} C\overline{\alpha}_s. \quad (6.4)$$

This extra contribution needs to be integrated up to roughly the binding energy $E_b \sim C^2 \overline{\alpha}_s^2 m$. This gives

$$\frac{\Delta\sigma^{\text{cont}}}{\sigma^{\text{cont}}} \sim \frac{1}{\sigma^{\text{cont}}} \int_{2m}^{2m+E_b} \Delta\hat{\sigma}^{\text{cont}}(\hat{s}) \, \mathrm{d}\sqrt{\hat{s}} \sim C^3 \overline{\alpha}_s^3 \sim \frac{\sigma^{\text{bound}}}{\sigma^{\text{cont}}}. \quad (6.5)$$

Thus for large $C\overline{\alpha}_s$ the continuum rate will also be proportionally larger, and there will never be more than $\sim 50\%$ annihilation decays (with $\overline{\alpha}_s \lesssim 1$).

In the more extreme limit in which the theory becomes strongly coupled and confining, the bound states will look just like simple resonances decaying either back into the standard model or within the strongly-coupled sector itself. But, in the regime of interest, when $\overline{\alpha}_s$ is perturbative but $(C\overline{\alpha}_s)^3$ is larger than for gluinonium, the binding particles will be observable on their own and the annihilation decays of their bound states will be significantly enhanced. In the next subsection we exemplify this with a toy model in which the particles are charged under an additional force.

6.2 Example model

Suppose there exist color adjoint fermions, like the gluino, which also transform under some representation R of a new SU(N) with a coupling constant α_N. Their pair production

processes will be like for the gluino, but without the contribution from virtual squarks. For $q\bar{q}$ initial states, only the anti-symmetric color adjoint state $\mathbf{8_A}$ is produced near the threshold. For gg initial states, pairs in the $\mathbf{1}$, $\mathbf{8_S}$ and $\mathbf{27}$ color configurations will be produced with relative cross sections $\hat{\sigma}_0(\mathbf{1}) : \hat{\sigma}_0(\mathbf{8_S}) : \hat{\sigma}_0(\mathbf{27}) = 1 : 2 : 3$ [8]. Since the initial states are $\mathrm{SU}(N)$ singlets, only $\mathrm{SU}(N)$-singlet configurations can be produced. Because of the sum over final states the rate is enhanced by an additional factor of the dimension of the representation, D_R.

For bound states, the cross-sections will also include the appropriate $|\psi(\mathbf{0})|^2$ factor for each color configuration. For computing those, note that the couplings in the potentials (2.1) are given by the simple replacements

$$C\,\overline{\alpha}_s \to C\,\overline{\alpha}_s + C_R\overline{\alpha}_N \,, \tag{6.6}$$

where C is the relevant QCD color factor from (3.9) for the $\mathbf{1}$, $\mathbf{8_S}$, $\mathbf{8_A}$ or $\mathbf{27}$ states, and C_R is the quadratic Casimir of the representation R of $\mathrm{SU}(N)$. For example, for the fundamental representation of $\mathrm{SU}(N)$, $D_R = N$ and $C_R = (N^2 - 1)/2N$, and for the adjoint representation $D_R = N^2 - 1$ and $C_R = N$.

To be explicit, the cross sections for the pseudoscalar bound states in the $(\mathbf{1}, \mathbf{1})$, $(\mathbf{8_S}, \mathbf{1})$ and $(\mathbf{27}, \mathbf{1})$ representations of $\mathrm{SU}(3)_{\mathrm{QCD}} \times \mathrm{SU}(N)$ will be like the cross section of the $\mathbf{1}$ gluinonium of the MSSM times the factors

$$D_R \left(\frac{3\,\overline{\alpha}_s + C_R\,\overline{\alpha}_N}{3\,\overline{\alpha}_s}\right)^3 , \quad 2D_R \left(\frac{3/2\,\overline{\alpha}_s + C_R\,\overline{\alpha}_N}{3\,\overline{\alpha}_s}\right)^3 , \quad 3D_R \left(\frac{-\overline{\alpha}_s + C_R\,\overline{\alpha}_N}{3\,\overline{\alpha}_s}\right)^3 , \quad (6.7)$$

respectively. The $(\mathbf{8_A}, \mathbf{1})$ vector will be like the $\mathbf{8_A}$ gluinonium times

$$D_R \left(\frac{3/2\,\overline{\alpha}_s + C_R\,\overline{\alpha}_N}{3/2\,\overline{\alpha}_s}\right)^3 . \tag{6.8}$$

Notice that even in relatively small representations and with order 1 values of $\overline{\alpha}_N/\overline{\alpha}_s$ the annihilation decay rates will be orders of magnitude larger than anything in the MSSM.

Figure 11 compares the dijet rates through annihilation decay to the CMS dijet search reach for several toy models, including the one with the MSSM gluino. Even when the additional force has the same strength as QCD ($\overline{\alpha}_N = \overline{\alpha}_s$), the cross section is enhanced by more than a factor of 10 if our "gluinos" are charged under the fundamental representation of a new $\mathrm{SU}(3)$ group. If they are charged under the adjoint of a new $\mathrm{SU}(4)$, the enhancement is almost 1000. If the new force is somewhat stronger, $\overline{\alpha}_N = 3\overline{\alpha}_s$ (which corresponds to a confinement scale of about $\Lambda_N \sim 10\,\mathrm{GeV}$, assuming for simplicity the same running as in QCD), the signal will be 10000 times larger than the annihilation decay signal from MSSM gluinonia.

The bound states may also annihilate into hidden sector dijets. But note that if the QCD and hidden sector couplings are comparable, the branching ratio into QCD dijets will still be of order 1, and the dijet rate will still have an enormous enhancement over annihilation decay rates in the MSSM. The phenomenology of decays into the hidden sector is very interesting, but model dependent, so we will not consider it here. In summary, there
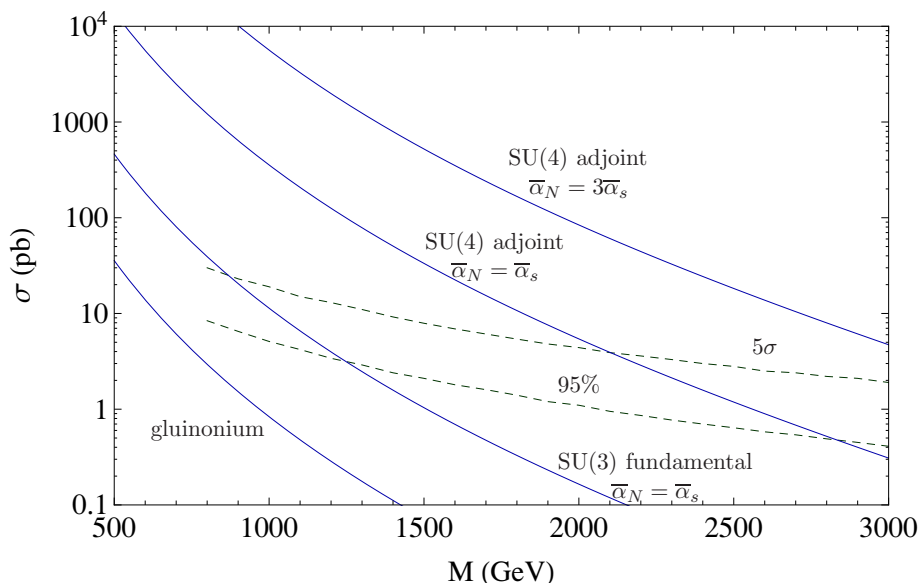
Figure 11. Dijet search reach (95% CL exclusion and 5σ discovery) with 100 pb⁻¹ at CMS [40], the MSSM gluinonium signal, and several models in which the particles are bound also by new forces.

is plenty of parameter space for complete models of this kind which are consistent with the various experimental bounds, in which such annihilation decays can provide spectacular signals at the LHC.

7 Summary and conclusions

In this paper we have considered the annihilation decays of a variety of possible bound state particles at the LHC. A number of examples were discussed at length, including bound states of top quarks, toponium, and bound states of gluinos, gluinonium. We also discussed bound states of squarks, squarkonium, and bound states associated with possible new strong forces. We have discussed how the spins and color representations of the particles determine the possible bound states, what determines their production channels and their cross sections, and how the mass spectrum of the model determines whether the bound states form and whether they decay by annihilation or through single-particle decays. Whenever the observation of the annihilation signal (or its absence) is feasible, it can provide valuable direct or indirect information about the underlying particles.

In the first and only standard model case, toponium, we found that the width of the top quark itself precludes any reasonable hope of finding toponium. Not only does the top's relatively large width force the top quark to decay much faster than it can annihilate, but it even decays too fast for a well-defined bound state to form, broadening the annihilation decay spectrum. There is no sharp distinction between the dijets coming from toponium annihilation decays and the contribution that virtual top quarks give to continuum dijet production. One might have also hoped to find evidence for toponium from the detailed

spectrum of the weak decay products, but since there is no sharp feature at the $t\bar{t}$ spectrum, the resolution required is beyond the ability of the LHC.

Although the top lifetime is fixed, gluinos may live long enough for the gluinonium to decay predominantly by annihilation in certain regions of parameter space, including some of the standard SPS points. We found that gluinonia may have substantial decay rates both to dijets and to $t\bar{t}$, and that both of these decay modes, although difficult to see, may be detectable at the LHC if the gluino mass is of the order of several hundred GeV. Looking at the mass distributions we found that both channels could provide peaks for mass determination. Moreover, the angular distributions in the dijet channel may help determine the spins of the resonances and thereby put constraints on the properties of the binding particle. However, due to the low signal-to-background ratio it will be challenging to extract spin information from the data.

For the case of bound squarks, squarkonium, observing annihilation decays into either dijets or $t\bar{t}$ pairs is practically impossible. First of all, despite the fact that the production is through gluon fusion, squarkonia cross sections are always several orders of magnitude smaller than gluinonia cross sections because of color factors. Moreover, for generic models, the squarks, like the top, will decay too fast relative to the rate of the annihilation processes or even before they form bound states, and the large width will smear the bound state resonance signal. Only stops may have a long enough lifetime so that the annihilation decay signal might possibly be seen. For these the best hope is using the small branching ratio to annihilate into two photons. Although the cross section for these decays is less than $1\,\mathrm{fb}$ for stop masses above $200\,\mathrm{GeV}$, this channel may be feasible for high luminosity. In fact, this channel might even be feasible for the gluinonium because of its large color factors even though the gluinos can annihilate into two photons only through loop diagrams. We also considered bound states of a squark and a gluino and two squarks (as opposed to a squark-anti-squark). Neither of these have visible annihilation decay signals.

Finally, we looked at annihilation decay cross sections in models with new forces. With a new confining force, the rate for annihilation decays may easily be much larger than in the supersymmetric models which only bind with QCD. There is a huge space of possible models, and just restricting to one simple class, we found that the signals for decays of these bound states are easy to see. Of course, in the limit that the new force is infinitely strong, the annihilation decays are just decays of a new resonance. However, in intermediate regimes it is easy to have both annihilation decays and other signatures, so that the annihilation decays provide complementary information.

Overall, it seems that annihilation decays of particles bound through QCD are difficult, but possible, to see, while particles bound through stronger forces will show up quickly. If the binding is not too strong, as with QCD, we will almost certainly have information about other decays of the constituent particles before we find the bound states. This will be useful in directing our search — knowing the mass ahead of time can improve the search strategy, especially in the dijet channel. Conversely, if the binding is very strong, exploring what the resonance may be a bound state of may help direct searches for other physics associated with the binding particles. In general, annihilation decays of bound states have the potential to provide an additional handle on the new physics we are likely to see at the LHC.

Acknowledgments

A Bound state formalism

For computing the bound-state effects, as well as finite-width effects, it is useful to consider the Green's function $G(\mathbf{x}, E)$ of the Schrödinger equation describing the two-particle system:[5]

$$\left[-\frac{\nabla^2}{m} + V(r) - E \right] G(\mathbf{x}, E) = \delta^{(3)}(\mathbf{x}), \tag{A.1}$$

where $E = \sqrt{\hat{s}} - 2m$. For zero angular momentum, the solution is [14]

$$G(\mathbf{0}, E) = -\frac{m^2}{4\pi} \left[\sqrt{-\frac{E}{m}} - C\overline{\alpha}_s \left[\ln\left(\frac{|C|\overline{\alpha}_s}{2} \sqrt{-\frac{m}{E}} \right) - F\left(1 - \frac{C\overline{\alpha}_s}{2} \sqrt{-\frac{m}{E}} \right) - \gamma_E \right] \right]$$

$$= -\frac{m^2}{4\pi} \left[\sqrt{-\frac{E}{m}} - C\overline{\alpha}_s \ln\left(\frac{|C|\overline{\alpha}_s}{2} \sqrt{-\frac{m}{E}} \right) - \frac{2}{\sqrt{m}} \sum_{n=1}^{\infty} \frac{E_n}{\sqrt{-E} - \text{sign}(C)\sqrt{E_n}} \right] \tag{A.2}$$

where $F(x) = \Gamma'(x)/\Gamma(x)$ is the digamma function, $\gamma_E = -F(1) \simeq 0.577$ is Euler's constant, C is the color factor (2.2) and $E_n = C^2 \overline{\alpha}_s^2 m/4n^2$ are the energies of the radial excitations. The solution describes both the bound states and the near-threshold continuum. Particles with width Γ (which gives width 2Γ to the bound states) are described by $E \to E + i\Gamma$ [14, 63].

A.1 Production cross section

By the optical theorem, the production cross section will be proportional to $\text{Im}\, G(\mathbf{0}, E)$, thus it can be written as [14, 63–66]

$$\hat{\sigma}(E) = \hat{\sigma}_0(E) \frac{\text{Im}\, G(\mathbf{0}, E)}{\text{Im}\, G_0(\mathbf{0}, E)}, \tag{A.3}$$

where $\hat{\sigma}_0$ is production cross section of the pair of particles (in the particular angular momentum and color representation) without the binding corrections and G_0 is the free Green's function, that is (A.2) with $C = 0$ (and $\Gamma = 0$), namely

$$G_0(\mathbf{0}, E) = -\frac{m^2}{4\pi} \sqrt{-\frac{E}{m}}, \qquad \text{Im}\, G_0(\mathbf{0}, E) = \frac{m^2}{4\pi} \sqrt{\frac{E}{m}}\, \theta(E) \simeq \frac{m^2}{4\pi} \beta\, \theta(E), \tag{A.4}$$

---

[5]Here $\mathbf{x}$ is the distance between the particles and we will be interested in $G(\mathbf{x} = \mathbf{0}, E)$ because we want to create the particles at zero separation and annihilate them at zero separation at a later time (the time is represented by its Fourier variable E).

where $\beta \equiv \sqrt{1 - 4m^2/\hat{s}}$ is the velocity of the particles in their center-of-mass frame. Then

$$\hat{\sigma}(E) = \frac{4\pi}{m^2} \frac{\hat{\sigma}_0(E)}{\beta} \operatorname{Im} G(\mathbf{0}, E) = \frac{\hat{\sigma}_0(E)}{2m^2 \Phi_2(E)} \operatorname{Im} G(\mathbf{0}, E) \,, \tag{A.5}$$

where we wrote the last expression in terms of the 2-particle phase space

$$\Phi_2 = \int \frac{\mathrm{d}^3 p_1}{(2\pi)^3 \, 2p_1^0} \int \frac{\mathrm{d}^3 p_2}{(2\pi)^3 \, 2p_2^0} \, (2\pi)^4 \delta^3 \left(\mathbf{p}_2 - \mathbf{p}_1\right) \delta \left(m\beta^2 - \frac{\mathbf{p}_1^2}{2m} - \frac{\mathbf{p}_2^2}{2m}\right) = \frac{\beta}{8\pi} \tag{A.6}$$

since the combination $\hat{\sigma}_0/\Phi_2$ remains well-behaved as we go below threshold.

For an attractive potential $(C > 0)$, the last term of (A.2) grows large near the bound state energies $E = -E_n$ if $E_n \gg \Gamma$:

$$G(\mathbf{0}, E) \simeq -\sum_n \frac{|\psi_n(\mathbf{0})|^2}{E + E_n + i\Gamma} \simeq -\sum_n \frac{2M_n |\psi_n(\mathbf{0})|^2}{\hat{s} - M_n^2 + 2iM_n\Gamma} \,, \tag{A.7}$$

$$\operatorname{Im} G(\mathbf{0}, E) \simeq \sum_n |\psi_n(\mathbf{0})|^2 \frac{\Gamma}{(E + E_n)^2 + \Gamma^2} \simeq \sum_n |\psi_n(\mathbf{0})|^2 \frac{4M_n^2 \Gamma}{(\hat{s} - M_n^2)^2 + 4M_n^2 \Gamma^2} \,, \tag{A.8}$$

where $|\psi_n(\mathbf{0})|^2 = C^3 \overline{\alpha}_s^3 m^3/(8\pi n^3)$ refers to the hydrogen-like wavefunctions describing the bound states and $M_n = 2m - E_n$ are their masses. In the limit $\Gamma \to 0$,

$$\operatorname{Im} G(\mathbf{0}, E) = \pi \sum_n |\psi_n(\mathbf{0})|^2 \, \delta(E + E_n) = \sum_n M_n |\psi_n(\mathbf{0})|^2 \, \Phi_1 \,, \tag{A.9}$$

$$\hat{\sigma}(E) = \frac{8\pi}{m} \frac{\hat{\sigma}_0(E)}{\beta} \sum_n |\psi_n(\mathbf{0})|^2 \, \Phi_1 = \sum_n \frac{|\psi_n(\mathbf{0})|^2}{m} \, \hat{\sigma}_0(E) \, \frac{\Phi_1}{\Phi_2} \,, \tag{A.10}$$

where $\Phi_1 = 2\pi \, \delta(\hat{s} - M_n^2)$ is the usual single-particle phase space. The last expression makes the agreement of the whole formalism with (3.5) manifest.[6] However, (3.5) is more general since it holds also for non-Coulombic potentials (but it is valid only for narrow bound states).

More generally, the imaginary part of (A.2) is [14, 64, 66]

$$\operatorname{Im} G(\mathbf{0}, E) = \frac{m^2}{4\pi} \left[v_+ + C\overline{\alpha}_s \tan^{-1}\left(\frac{v_+}{v_-}\right) + \sum_{n=1}^{\infty} E_n \frac{C\overline{\alpha}_s \Gamma/n + 2v_+ \left(\sqrt{E^2 + \Gamma^2} + E_n\right)}{(E + E_n)^2 + \Gamma^2} \right] \,, \tag{A.11}$$

where

$$v_{\pm} = \sqrt{\frac{\sqrt{E^2 + \Gamma^2} \pm E}{2m}} \,. \tag{A.12}$$

To see what (A.11) means, suppose $\Gamma \to 0$. For $E < 0$, eq. (A.11) reduces to a sum of narrow Breit-Wigners (A.8) in the attractive case and vanishes in the repulsive case. For $E > 0$:

$$\operatorname{Im} G(\mathbf{0}, E) = \frac{C\overline{\alpha}_s m^2}{4} \frac{1}{1 - \exp\left(-\pi C\overline{\alpha}_s/\beta\right)} \,. \tag{A.13}$$

---

[6]In the case that the two particles are identical, Φ_2 in (A.6) will actually be twice the phase space. This is consistent with the factor of $1/2$ discussed after (3.6).

For a repulsive potential, the imaginary part (A.13) is suppressed to zero at the naïve threshold $E = 0$, but for an attractive potential it starts with a finite value

$$\text{Im}\, G(\mathbf{0}, E \to 0^+) = \frac{C \overline{\alpha}_s m^2}{4}\,. \tag{A.14}$$

at the threshold.

A.2 Annihilation processes

Consider the process

$$ab \to \alpha\beta \to AB\,. \tag{A.15}$$

When $\alpha\beta$ form a narrow bound state, the standard resonance production formula (B.6) gives

$$\hat{\sigma}_{ab \to (\alpha\beta) \to AB}(\hat{s}) = \frac{4\pi\,(2J+1)\,D_{(\alpha\beta)}}{D_a D_b} \frac{\Gamma_{(\alpha\beta) \to ab}\,\Gamma_{(\alpha\beta) \to AB}}{(\hat{s} - M^2)^2 + \hat{s}\,\Gamma^2} \qquad [\,\times 2 \quad \text{if} \quad a = b\,]\,, \tag{A.16}$$

where $M \simeq 2m$ is the mass and J is the spin of the bound state and D_x denotes the dimension of the color representation of the particle x.

When the bound state is not narrow or we want to obtain the contribution from the near-threshold $\alpha\beta$ continuum as well, we can use the fact that $G(\mathbf{0}, E)$ is the two-point function describing the pair, so the matrix element (squared) is proportional to $|G(\mathbf{0}, E)|^2$, while all the short-distance factors can be taken from the narrow bound state case. Dividing (A.16) by the narrow-width $|G(\mathbf{0}, E)|^2$ from (A.7)[7] and multiplying by the general $|G(\mathbf{0}, E)|^2$ we obtain

$$\hat{\sigma}_{ab \to \alpha\beta \to AB}(E) = \frac{\pi\,(2J+1)\,D_{(\alpha\beta)}}{D_a D_b} \frac{\Gamma_{(\alpha\beta) \to ab}\,\Gamma_{(\alpha\beta) \to AB}}{4m^2 |\psi(\mathbf{0})|^4}\,|G(\mathbf{0}, E)|^2 \quad [\,\times 2 \text{ if } a = b\,]\,. \tag{A.17}$$

Note that $|\psi(\mathbf{0})|^4$ in the denominator cancels the $|\psi(\mathbf{0})|^2$ factors in the annihilation rates, so the prefactor of $|G(\mathbf{0}, E)|^2$ in (A.17) depends only on the short-distance physics. We can see this more explicitly by comparing (A.10) and (B.8)[8] which allows us to express the bound state annihilation rates in terms of production cross sections of free particles, giving

$$\hat{\sigma}_{ab \to \alpha\beta \to AB}(E) = \frac{D_A D_B}{4\pi\,(2J+1)\,D_{(\alpha\beta)}m^2} \frac{\hat{\sigma}_0^{ab \to \alpha\beta}(E)}{\Phi_2} \frac{\hat{\sigma}_0^{AB \to \alpha\beta}(E)}{\Phi_2}\,|G(\mathbf{0}, E)|^2 \quad \left[\,\times \frac{1}{2} \text{ if } A = B\,\right] \tag{A.18}$$

Written in this form, the expression is useful also for color representations that do not bind.

For the bound states in the narrow-width limit, (A.7) and (A.8) show that

$$|G(\mathbf{0}, E)|^2 = \frac{|\psi(\mathbf{0})|^2}{\Gamma}\,\text{Im}\, G(\mathbf{0}, E) \to \frac{|\psi(\mathbf{0})|^2}{\Gamma_{\text{tot}}/2}\,\text{Im}\, G(\mathbf{0}, E)\,, \tag{A.19}$$

---

[7]More specifically, $|G(\mathbf{0}, E)|^2$ from (A.7) includes the interference with the radial excitations, which we should have, in principle, included in (A.16) as well. We ignore this for simplicity of presentation.

[8]This expression applies if A and B are massless particles with 2 polarizations, but can be easily generalized.

where in the last step we promoted the decay rate to include not just the constituent particle widths Γ but also the (sum of all the) annihilation rates Γ_{ann}:

$$\Gamma_{\text{tot}} = 2\,\Gamma + \Gamma_{\text{ann}}\,. \tag{A.20}$$

This makes sense because then (A.17) or (A.18) reduces to a branching ratio times the production cross section (A.5):

$$\hat{\sigma}_{ab\to\alpha\beta\to AB}(E) = \frac{\Gamma_{(\alpha\beta)\to AB}}{\Gamma_{\text{tot}}} \cdot \hat{\sigma}_0^{ab\to\alpha\beta}(E)\,\frac{\operatorname{Im} G(\mathbf{0}, E)}{2m^2\,\Phi_2}\,. \tag{A.21}$$

When the constituent particle width Γ is not much smaller than the binding energy E_b, $|G(\mathbf{0}, E)|^2$ is no longer proportional to $\operatorname{Im} G(\mathbf{0}, E)$ so the branching ratio is not simply determined by $\Gamma_{(\alpha\beta)\to AB}/\Gamma_{\text{tot}}$. In fact, the annihilation rates are not even well-defined in this situation because the bound states are not well-defined. Nevertheless, we can still use (A.18).

However, this method cannot be used when the annihilation rate Γ_{ann} is the one that becomes comparable to E_b, because the width Γ in this formalism is the single-particle decay width, without taking into account the possibility of annihilation (see, e.g., the derivations in [14, 63]). But this regime will not usually be relevant to actual systems because of (3.1).

Let us now study the behavior in the continuum. Note that for $|E|, \Gamma \lesssim E_b$ we can approximate (A.2) by

$$G(\mathbf{0}, E) \simeq -\frac{C\overline{\alpha}_s m^2}{4\pi}\left[\pi \cot\left(\frac{\pi C\overline{\alpha}_s}{2}\sqrt{-\frac{m}{E}}\right) + \gamma_E\right]. \tag{A.22}$$

For $E > 0$ this is

$$G(\mathbf{0}, E) \simeq -\frac{C\overline{\alpha}_s m^2}{4\pi}\left[-i\pi \coth\left(\frac{\pi C\overline{\alpha}_s}{2}\sqrt{\frac{m}{E}}\right) + \gamma_E\right] \simeq -\frac{C\overline{\alpha}_s m^2}{4\pi}\left(\gamma_E - i\pi\right), \tag{A.23}$$

which gives

$$|G(\mathbf{0}, E)|^2 \simeq \frac{C^2\overline{\alpha}_s^2 m^4}{16\pi^2}\left(\gamma_E^2 + \pi^2\right). \tag{A.24}$$

Using (A.18) with (A.24) and (A.5) with (A.14), we obtain the branching ratio of the annihilation-like processes in the near-threshold continuum:

$$\frac{\hat{\sigma}_{ab\to\alpha\beta\to AB}}{\hat{\sigma}_{ab\to\alpha\beta}} \simeq \frac{\gamma_E^2 + \pi^2}{8\pi^3}\,C\overline{\alpha}_s\,\frac{D_A D_B}{(2J+1)D_{\alpha\beta}}\frac{\hat{\sigma}_0^{AB\to\alpha\beta}}{\Phi_2}m^2 \quad \left[\times\frac{1}{2}\ \text{if}\ A = B\right]. \tag{A.25}$$

With typical strong-interaction diagrams we will have $\hat{\sigma}_0^{AB\to\alpha\beta}/\Phi_2 \sim \alpha_s^2/m^2$ giving

$$\frac{\hat{\sigma}_{ab\to\alpha\beta\to AB}}{\hat{\sigma}_{ab\to\alpha\beta}} \sim C\overline{\alpha}_s\alpha_s^2 \sim 10^{-3}\,. \tag{A.26}$$

A.3 The case of $t\bar{t}$

Let us apply the results of this appendix to computing the curves in figure 1. The near-threshold tree-level $t\bar{t}$ production cross sections in the various spin and color channels are (see, e.g., [67])

$$\left\{ \hat{\sigma}_0^{gg \to {}^1S_0(\mathbf{1})} \, , \ \hat{\sigma}_0^{gg \to {}^1S_0(\mathbf{8})} \, , \ \hat{\sigma}_0^{q\bar{q} \to {}^3S_1(\mathbf{8})} \right\} = \left\{ \frac{1}{96} \, , \ \frac{5}{192} \, , \ \frac{1}{9} \right\} \times \frac{\pi \alpha_s^2}{m_t^2} \beta \, . \tag{A.27}$$

From (A.5), the production cross sections for these three channels are

$$\hat{\sigma}(E) = \frac{4\pi^2 \alpha_s^2}{m_t^4} \times \left\{ \frac{1}{96} \operatorname{Im} G^{\mathbf{1}}(\mathbf{0}, E) \, , \ \frac{5}{192} \operatorname{Im} G^{\mathbf{8}}(\mathbf{0}, E) \, , \ \frac{1}{9} \operatorname{Im} G^{\mathbf{8}}(\mathbf{0}, E) \right\} \, , \tag{A.28}$$

and from (A.18) the annihilation cross sections (for $A, B = a, b$) are

$$\hat{\sigma}^{\mathrm{ann}}(E) = \frac{\pi^3 \alpha_s^4}{m_t^6} \times \left\{ \frac{1}{18} \left| G^{\mathbf{1}}(\mathbf{0}, E) \right|^2 \, , \ \frac{25}{576} \left| G^{\mathbf{8}}(\mathbf{0}, E) \right|^2 \, , \ \frac{2}{27} \left| G^{\mathbf{8}}(\mathbf{0}, E) \right|^2 \right\} \, . \tag{A.29}$$

In practice, when the potential is repulsive $|G(\mathbf{0}, E)|^2$ is highly suppressed in the near-threshold region, so only the color-singlet contributes to the annihilation signal in the case of $t\bar{t}$ pairs.

For the near-threshold continuum, just for the color-singlet, (A.25) gives the branching ratio

$$\frac{\hat{\sigma}_{gg \to t\bar{t} \to gg}}{\hat{\sigma}_{gg \to t\bar{t}}} \simeq \frac{\gamma_E^2 + \pi^2}{3\pi} C \overline{\alpha}_s \alpha_s^2 = 2.4 \times 10^{-3} \, . \tag{A.30}$$

B Resonance cross sections from decay rates

Consider the process

$$a \, b \to M_\Gamma \to A \, B \ldots \, , \tag{B.1}$$

in which partons a and b (quarks or gluons) produce a resonance of mass M, width Γ, spin J, in a specific color representation, that then decays into particles A and B (or more). The resonance propagator contributes the denominator

$$\frac{1}{(\hat{s} - M^2)^2 + M^2 \Gamma^2} \, . \tag{B.2}$$

The tensor structure of the propagator can be written as a sum of products of polarization vectors which will be absorbed in the decay rates that we will now discuss. The final part of the process (B.1) is the same as in the decay $M \to A \, B$ (by rotational invariance, the total decay rate is the same for every polarization of M), so it contributes

$$2M \, \Gamma_{M \to AB} \, . \tag{B.3}$$

Similarly, the initial part of the squared matrix element, summed (for the purpose of the derivation) over all possible directions for the incoming particles and over the polarizations of a, b and M, is proportional to $\Gamma_{M \to ab}$. It is given by

$$\frac{(2J + 1) D_M}{2D_a \cdot 2D_b} \frac{4\pi}{\hat{s}} 2M \, \Gamma_{M \to ab} \qquad [\, \times 2 \quad \text{if} \quad a = b \,] \, . \tag{B.4}$$

where we undid the integration over the different directions (which is trivial after summing over the polarizations), denoted the dimension of the color representation of X by D_X, and assumed a and b to have two helicities. This gives

$$\hat{\sigma}_{ab \to M \to AB}(\hat{s}) = \frac{4\pi \, (2J+1) \, D_M}{D_a D_b} \frac{M^2}{\hat{s}} \frac{\Gamma_{M \to ab} \, \Gamma_{M \to AB}}{\left(\hat{s} - M^2\right)^2 + M^2 \Gamma^2} \qquad [\, \times 2 \quad \text{if} \quad a = b \,] \, . \quad \text{(B.5)}$$

We should note, however, that the actual mass of the resonance is $\sqrt{\hat{s}}$ rather than M, and we need to make this replacement throughout the calculation:

$$\hat{\sigma}_{ab \to M \to AB}(\hat{s}) = \frac{4\pi \, (2J+1) \, D_M}{D_a D_b} \frac{\Gamma_{M \to ab} \, \Gamma_{M \to AB}}{\left(\hat{s} - M^2\right)^2 + \hat{s} \, \Gamma^2} \qquad [\, \times 2 \quad \text{if} \quad a = b \,] \, , \quad \text{(B.6)}$$

where the widths $\Gamma_{M \to ab}$, $\Gamma_{M \to AB}$ and Γ should be evaluated assuming resonance mass $\sqrt{\hat{s}}$ instead of M. In the narrow-width limit $\Gamma \ll M$, (B.6) becomes

$$\hat{\sigma}_{ab \to M \to AB}(\hat{s}) \simeq \frac{2\pi \, (2J+1) \, D_M}{D_a D_b} \frac{\Gamma_{M \to ab} \, \Gamma_{M \to AB}}{M \, \Gamma} \, 2\pi \, \delta(\hat{s} - M^2) \qquad [\, \times 2 \quad \text{if} \quad a = b \,] \, , \quad \text{(B.7)}$$

and if we further sum over all the possible final states in (B.1) this simplifies to

$$\hat{\sigma}_{ab \to M}(\hat{s}) \simeq \frac{2\pi \, (2J+1) \, D_M}{D_a D_b} \frac{\Gamma_{M \to ab}}{M} \, 2\pi \, \delta(\hat{s} - M^2) \qquad [\, \times 2 \quad \text{if} \quad a = b \,] \, . \quad \text{(B.8)}$$

As expected, the production cross section is independent of the available decay modes.

C Algorithm for $t\bar{t}$ reconstruction

This is the algorithm we use for the reconstruction of the $t\bar{t}$ pair in the semileptonic channel with an electron or a muon. It includes the most essential features of the algorithms studied by ATLAS [68] and CMS [39]. The efficiencies given below were obtained for signals of scalar and vector $600\,\mathrm{GeV}$ resonances and the standard model background that was described in section 4.1. The efficiencies are listed in the order scalar/vector/background.

1. We select events with exactly one electron or muon with $p_T > 35\,\mathrm{GeV}$ and rapidity $|y| < 2.5$. Efficiency: 30%/28%/22%.

2. We save all jets with $p_T > 20\,\mathrm{GeV}$, but require to have at least 4 jets with $p_T > 30\,\mathrm{GeV}$. Efficiency: 75%/57%/64%.

3. We require that the 4 hardest jets have rapidities $|y| < 2.5$. Efficiency: 75%/75%/67%.

4. We start with reconstructing the leptonically decaying top. We compute the transverse momentum of the neutrino from the transverse momenta of the lepton and all the jets. By requiring W to be on-shell, we obtain a quadratic equation for the longitudinal momentum of the neutrino, and keep both solutions. If the discriminant is negative, we try reducing neutrino's transverse momentum by up to 15% till the solution is possible. Efficiency: 76%/79%/76% (neutrino momentum reduction was used in 7%/7%/8% of these cases).

5. We then find which of the jets best reproduces the mass of the top when combined with the W. We choose the neutrino momentum assignment that gives the better top mass accuracy. We require top mass accuracy of at least 10%. Efficiency: 87%/87%/88%.

6. To reconstruct the hadronically decaying top, we take the remaining jets and find the assignment of three of them that reconstructs the W and the top most successfully, based on the criterion of minimizing the quantity

$$e \equiv \sqrt{\left(\frac{\Delta m_W}{0.1 m_W}\right)^2 + \left(\frac{\Delta m_t}{0.2 m_t}\right)^2},$$ (C.1)

where Δm_W and Δm_t are the differences between the reconstructed and the actual masses. We require that the best assignment has $e = e_{\text{best}} < \sqrt{2}$ (efficiency: 47%/41%/46%) and the next-to-best assignment has $e > 3\, e_{\text{best}}$ (efficiency: 24%/34%/26%).

7. To eliminate many of the events that were not reconstructed correctly, we require that the azimuthal angle ϕ between the two tops is at least 160° (efficiency: 48%/67%/46%).

The fraction of events that remains at the end of the algorithm is 0.6%/0.8%/0.34% out of all the $t\bar{t}$ events.

References

[1] J.T. Goldman and H. Haber, *Gluinonium: the hydrogen atom of supersymmetry*, *Physica* **15 D** (1985) 181 [SPIRES].

[2] W.-Y. Keung and A. Khare, *Two-gluino bound states*, *Phys. Rev.* **D 29** (1984) 2657 [SPIRES].

[3] J.H. Kuhn and S. Ono, *Production and decay of gluino-gluino bound states*, *Phys. Lett.* **B 142** (1984) 436 [SPIRES].

[4] E. Chikovani, V. Kartvelishvili, R. Shanidze and G. Shaw, *Bound states of two gluinos at the Tevatron and CERN LHC*, *Phys. Rev.* **D 53** (1996) 6653 [hep-ph/9602249] [SPIRES].

[5] E. Bouhova-Thacker, V. Kartvelishvili and A. Small, *Search for gluino gluino bound states*, *Nucl. Phys. Proc. Suppl.* **133** (2004) 122 [SPIRES].

[6] E. Bouhova-Thacker, V. Kartvelishvili and A. Small, *Search for gluino-gluino bound states with ATLAS*, *Nucl. Phys. Proc. Suppl.* **152** (2006) 300 [SPIRES].

[7] K. Cheung and W.-Y. Keung, *Split supersymmetry, stable gluino and gluinonium*, *Phys. Rev.* **D 71** (2005) 015015 [hep-ph/0408335] [SPIRES].

[8] K. Hagiwara and H. Yokoya, *Bound-state effects on gluino-pair production at hadron colliders*, *JHEP* **10** (2009) 049 [arXiv:0909.3204] [SPIRES].

[9] M.R. Kauth, J.H. Kuhn, P. Marquard and M. Steinhauser, *Gluinonia: energy levels, production and decay*, *Nucl. Phys.* **B 831** (2010) 285 [arXiv:0910.2612] [SPIRES].

[10] B.C. Allanach et al., *The Snowmass points and slopes: benchmarks for SUSY searches*, *Eur. Phys. J.* **C 25** (2002) 113 [hep-ph/0202233] [SPIRES].

[11] H. Baer, K.-m. Cheung and J.F. Gunion, *A heavy gluino as the lightest supersymmetric particle*, *Phys. Rev.* **D 59** (1999) 075002 [`hep-ph/9806361`] [SPIRES].

[12] S. Raby and K. Tobe, *The phenomenology of SUSY models with a gluino LSP*, *Nucl. Phys.* **B 539** (1999) 3 [`hep-ph/9807281`] [SPIRES].

[13] N. Arkani-Hamed and S. Dimopoulos, *Supersymmetric unification without low energy supersymmetry and signatures for fine-tuning at the LHC*, *JHEP* **06** (2005) 073 [`hep-th/0405159`] [SPIRES].

[14] V.S. Fadin and V.A. Khoze, *Production of a pair of heavy quarks in e^+e^- annihilation in the threshold region*, *Sov. J. Nucl. Phys.* **48** (1988) 309 [SPIRES].

[15] M. Beneke, A. Signer and V.A. Smirnov, *Top quark production near threshold and the top quark mass*, *Phys. Lett.* **B 454** (1999) 137 [`hep-ph/9903260`] [SPIRES].

[16] Y. Kiyo, J.H. Kuhn, S. Moch, M. Steinhauser and P. Uwer, *Top-quark pair production near threshold at LHC*, *Eur. Phys. J.* **C 60** (2009) 375 [`arXiv:0812.0919`] [SPIRES].

[17] J.H. Kuhn and P.M. Zerwas, *The toponium scenario*, *Phys. Rept.* **167** (1988) 321 [SPIRES].

[18] K. Hagiwara, Y. Sumino and H. Yokoya, *Bound-state effects on top quark production at hadron colliders*, *Phys. Lett.* **B 666** (2008) 71 [`arXiv:0804.1014`] [SPIRES].

[19] J.H. Kuhn and E. Mirkes, *Toponium production at hadron colliders*, *Phys. Lett.* **B 296** (1992) 425 [SPIRES].

[20] J.H. Kuhn and E. Mirkes, *QCD corrections to toponium production at hadron colliders*, *Phys. Rev.* **D 48** (1993) 179 [`hep-ph/9301204`] [SPIRES].

[21] N. Fabiano, A. Grau and G. Pancheri, *Observability limits for toponium at hadron colliders*, *Phys. Rev.* **D 50** (1994) 3173 [SPIRES].

[22] R.M. Barnett, J.F. Gunion and H.E. Haber, *Gluino decay patterns and signatures*, *Phys. Rev.* **D 37** (1988) 1892 [SPIRES].

[23] M. Toharia and J.D. Wells, *Gluino decays with heavier scalar superpartners*, *JHEP* **02** (2006) 015 [`hep-ph/0503175`] [SPIRES].

[24] W. Kilian, T. Plehn, P. Richardson and E. Schmidt, *Split supersymmetry at colliders*, *Eur. Phys. J.* **C 39** (2005) 229 [`hep-ph/0408088`] [SPIRES].

[25] J.L. Hewett, B. Lillie, M. Masip and T.G. Rizzo, *Signatures of long-lived gluinos in split supersymmetry*, *JHEP* **09** (2004) 070 [`hep-ph/0408248`] [SPIRES].

[26] M.E. Peskin and D.V. Schroeder, *An introduction to quantum field theory*. Westview Press, U.S.A. (1995), section 5.3.

[27] J.H. Kuhn, J. Kaplan and E.G.O. Safiani, *Electromagnetic annihilation of e^+e^- into quarkonium states with even charge conjugation*, *Nucl. Phys.* **B 157** (1979) 125 [SPIRES].

[28] V.A. Khoze, A.D. Martin and M.G. Ryskin, *Prospects for new physics observations in diffractive processes at the LHC and Tevatron*, *Eur. Phys. J.* **C 23** (2002) 311 [`hep-ph/0111078`] [SPIRES].

[29] P.J. Bussey, T.D. Coughlin, J.R. Forshaw and A.D. Pilkington, *Central exclusive production of longlived gluinos at the LHC*, *JHEP* **11** (2006) 027 [`hep-ph/0607264`] [SPIRES].

[30] G.T. Bodwin, E. Braaten and G.P. Lepage, *Rigorous QCD predictions for decays of P wave quarkonia*, *Phys. Rev.* **D 46** (1992) 1914 [`hep-lat/9205006`] [SPIRES].

[31] A. Kulesza and L. Motyka, *Soft gluon resummation for the production of gluino-gluino and squark-antisquark pairs at the LHC*, *Phys. Rev.* **D 80** (2009) 095004 [`arXiv:0905.4749`] [SPIRES].

[32] W. Beenakker, R. Hopker, M. Spira and P.M. Zerwas, *Squark and gluino production at hadron colliders*, *Nucl. Phys.* **B 492** (1997) 51 [hep-ph/9610490] [SPIRES].

[33] A.D. Martin, W.J. Stirling, R.S. Thorne and G. Watt, *Parton distributions for the LHC*, *Eur. Phys. J.* **C 63** (2009) 189 [arXiv:0901.0002] [SPIRES].

[34] T. Sjöstrand, S. Mrenna and P.Z. Skands, *PYTHIA 6.4 physics and manual*, *JHEP* **05** (2006) 026 [hep-ph/0603175] [SPIRES].

[35] T. Sjöstrand, S. Mrenna and P.Z. Skands, *A brief introduction to PYTHIA 8.1*, *Comput. Phys. Commun.* **178** (2008) 852 [arXiv:0710.3820] [SPIRES].

[36] http://home.thep.lu.se/~torbjorn/Pythia.html.

[37] G.P. Salam and G. Soyez, *A practical seedless infrared-safe cone jet algorithm*, *JHEP* **05** (2007) 086 [arXiv:0704.0292] [SPIRES].

[38] http://projects.hepforge.org/siscone/.

[39] CMS collaboration, *Study of the top-pair invariant mass distribution in the semileptonic muon channel at 10 TeV*, CMS-PAS-TOP-09-009.

[40] CMS collaboration, K. Gumus et al., *CMS sensitivity to dijet resonances*, CMS-NOTE-2006-070.

[41] G.P. Salam, *Towards jetography*, arXiv:0906.1833 [SPIRES].

[42] D.E. Kaplan, K. Rehermann, M.D. Schwartz and B. Tweedie, *Top tagging: a method for identifying boosted hadronically decaying top quarks*, *Phys. Rev. Lett.* **101** (2008) 142001 [arXiv:0806.0848] [SPIRES].

[43] FOR THE CMS collaboration, G. Giurgiu, *Reconstruction of high transverse momentum top quarks at CMS*, arXiv:0909.4894 [SPIRES].

[44] J. Thaler and L.-T. Wang, *Strategies to identify boosted tops*, *JHEP* **07** (2008) 092 [arXiv:0806.0023] [SPIRES].

[45] L.G. Almeida, S.J. Lee, G. Perez, I. Sung and J. Virzi, *Top jets at the LHC*, *Phys. Rev.* **D 79** (2009) 074012 [arXiv:0810.0934] [SPIRES].

[46] ATLAS collaboration, *Top quark properties*, ATL-PHYS-PUB-2009-044.

[47] S.P. Martin, *Diphoton decays of stoponium at the Large Hadron Collider*, *Phys. Rev.* **D 77** (2008) 075002 [arXiv:0801.0237] [SPIRES].

[48] S. Dawson, E. Eichten and C. Quigg, *Search for supersymmetric particles in hadron-hadron collisions*, *Phys. Rev.* **D 31** (1985) 1581 [SPIRES].

[49] M.J. Herrero, A. Mendez and T.G. Rizzo, *Production of heavy squarkonium at high-energy pp colliders*, *Phys. Lett.* **B 200** (1988) 205 [SPIRES].

[50] M. Drees and M.M. Nojiri, *A new signal for scalar top bound state production*, *Phys. Rev. Lett.* **72** (1994) 2324 [hep-ph/9310209] [SPIRES].

[51] M. Drees and M.M. Nojiri, *Production and decay of scalar stoponium bound states*, *Phys. Rev.* **D 49** (1994) 4595 [hep-ph/9312213] [SPIRES].

[52] S.P. Martin and J.E. Younkin, *Radiative corrections to stoponium annihilation decays*, *Phys. Rev.* **D 80** (2009) 035026 [arXiv:0901.4318] [SPIRES].

[53] J.E. Younkin and S.P. Martin, *QCD corrections to stoponium production at hadron colliders*, arXiv:0912.4813 [SPIRES].

[54] P. Moxhay and R.W. Robinett, *Searching for scalar quarkonium at proton-anti-proton colliders*, *Phys. Rev.* **D 32** (1985) 300 [SPIRES].

[55] D.S. Gorbunov and V.A. Ilyin, *Stoponium search at photon linear collider*, *JHEP* **11** (2000) 011 [hep-ph/0004092] [SPIRES].

[56] V.D. Barger et al., *Superheavy quarkonium production and decays: a new Higgs signal*, *Phys. Rev.* **D 35** (1987) 3366 [*Erratum ibid.* **D 38** (1988) 1632] [SPIRES].

[57] E. Arik, O. Cakir, S.A. Cetin and S. Sultansoy, *Fourth generation pseudoscalar quarkonium production and observability at hadron colliders*, *Phys. Rev.* **D 66** (2002) 116006 [hep-ph/0208169] [SPIRES].

[58] C. Kim and T. Mehen, *Color octet scalar bound states at the LHC*, *Phys. Rev.* **D 79** (2009) 035011 [arXiv:0812.0307] [SPIRES].

[59] C.D. Carone, J.M. Conroy, M. Sher and I. Turan, *Universal extra dimensions and Kaluza Klein bound states*, *Phys. Rev.* **D 69** (2004) 074018 [hep-ph/0312055] [SPIRES].

[60] N. Fabiano and O. Panella, *Threshold production of meta-stable bound states of Kaluza Klein excitations in universal extra dimensions*, arXiv:0804.3917 [SPIRES].

[61] M.J. Strassler and K.M. Zurek, *Echoes of a hidden valley at hadron colliders*, *Phys. Lett.* **B 651** (2007) 374 [hep-ph/0604261] [SPIRES].

[62] J. Kang and M.A. Luty, *Macroscopic strings and 'quirks' at colliders*, *JHEP* **11** (2009) 065 [arXiv:0805.4642] [SPIRES].

[63] M.J. Strassler and M.E. Peskin, *The Heavy top quark threshold: QCD and the Higgs*, *Phys. Rev.* **D 43** (1991) 1500 [SPIRES].

[64] V.S. Fadin and V.A. Khoze, *Threshold behavior of heavy top production in e^+e^- collisions*, *Pis'ma Zh. Eksp. Teor. Fiz.* **46** (1987) 417 [*JETP Lett.* **46** (1987) 525] [SPIRES].

[65] V.S. Fadin, V.A. Khoze and N.G. Uraltsev, *Large B^0–$\overline{B}^0$ mixing and physics of the heavy t-quark*, presented at *Mtg. on Indirect Evidence of New Energy Scales from Low Energy Precision Experiments*, June 22-24, Trieste, (1987), available at http://www-lib.kek.jp/cgi-bin/img_index?200033095.

[66] V.S. Fadin, V.A. Khoze and T. Sjöstrand, *On the threshold behavior of heavy top production*, *Z. Phys.* **C 48** (1990) 613 [SPIRES].

[67] R. Bonciani, S. Catani, M.L. Mangano and P. Nason, *NLL resummation of the heavy-quark hadroproduction cross- section*, *Nucl. Phys.* **B 529** (1998) 424 [hep-ph/9801375] [SPIRES].

[68] ATLAS collaboration, E. Cogneras and D. Pallin, *Generic $t\bar{t}$ resonance search with the ATLAS detector*, ATL-PHYS-PUB-2006-033.